Chapter 3

Reactivity of Matrix-Isolated Tetrazolyl Derivatives: Photochemistry, Molecular Structure and Vibrational Spectra

In Chapter one, a brief description of the matrix isolation technique and discussion of its main advantages and drawbacks when applied to photochemical studies on organic molecules was presented.

In this Chapter, a general overview of the photochemistry of a series of matrix-isolated tetrazole derivatives and the general pattern of their photoreactions is presented. Several representative tetrazoles were trapped in a rigid environment of solidified argon, at cryogenic temperatures (typically 10 K) and subjected to *in situ* photolysis. The range of possible reactions of the isolated species was controlled by choice of the excitation wavelengths. FT-IR spectroscopy provided experimental frequencies and intensities of characteristic absorptions of the isolated chemical species, both for reagents and photoproducts. The analysis of experimental data was assisted by their direct comparison with the vibrational spectra theoretically calculated for the single molecule in vacuum. This comparison was facilitated because the inert matrix only slightly affects the structure of the isolated molecules, and also owing to the high resolution of infrared matrix spectra (a few tenths of cm^{-1}).

UV-excitation resulted in photofragmentation of the monomeric tetrazoles with a wide range of exit channels. Since the obtained fragments generally stay in the matrix cage where they are formed, no subsequent cross-reactions involving species resulting from photolysis of different reactant molecules can occur. As a result, by using FT-IR spectroscopy, it was possible to characterize a number of relatively unusual or highly reactive molecules, such as antiaromatic azirines, azides, cyanates, isocyanates, diazirenes or methylenimine, formed from photolysis of tetrazoles in the inert matrix. In some examples described in this Chapter, the spectroscopic characterization of these molecular species was presented for the first time.

In order to assist the reader on the interpretation of the vast number of results obtained during the studies of the photochemistry of matrix-isolated tetrazole derivatives, this Chapter is divided in three main parts, each one grouping structurally similar tetrazoles: *Part I* (5-Alkoxy-1-phenyl-tetrazoles), *Part II* (2-Methyl-2*H*-tetrazol-5-amine) and *Part III* (1-Phenyl-tetrazolones).

The work described in this Chapter is included in the following international scientific journals: *Journal of Physical Chemistry* A **2005**, *109*, 7967-7976, *Journal of Photochemistry and Photobiology A - Chemistry* **2006**, *179*, 243-255, *Journal of Photochemistry and Photobiology A - Chemistry* **2006**, *180*, 175-183, *Journal of Physical Chemistry A* **2007**, *111*, 2879-2888 and *Photochemical & Photobiological Sciences* **2007**, *6*, 1170-1176. The contents of these publications are partly reproduced below.

PART I:
Photochemistry and Vibrational Spectra of 5-Alkoxy-1-phenyl-tetrazoles

3.1.1. Introduction

The extensive applications of tetrazoles stimulated research in areas such as the reactivity of various tetrazolyl derivatives and the design of synthetic methodologies. Among the compounds investigated are 5-alkoxy-1-aryl-tetrazoles. Efficient and easy to carry synthetic methodologies to these compounds have been described.[1,2] 5-Alkoxy-1-aryl-tetrazoles are also important compounds from a synthetic view point because they act as intermediates to the preparation of 5-alkyl-1-aryl-4,5-dihydro-1*H*-tetrazol-5-ones *via* a thermally induced Chapmann isomerisation.[3,4]

In the past, very little attention has been given to the study of tetrazole-based compounds at a molecular level. Recently, a research program aiming to fill this gap was started in the *Laboratory of Molecular Cryospectroscopy and Biospectroscopy* of the *Coimbra Chemistry Centre*, at the University of Coimbra. Unsubstituted tetrazole[5] and some of its representative derivatives[6-11] were studied under this program. In these studies, the molecular structure, tautomerism, vibrational spectra and photochemistry of tetrazoles were investigated by a concerted approach using matrix isolation infrared spectroscopy and high-level DFT-based theoretical calculations. Regarding their photochemistry, tetrazoles have been found to be extremely interesting and challenging molecules. Most of times, several UV-induced processes occur simultaneously and the relative importance of each one has been shown to be strongly dependent on the substituents of the tetrazole ring.[8-15]

In this part, results on the molecular structure, vibrational spectra and photochemistry of two matrix-isolated 5-alkoxy-1-phenyl-1*H*-tetrazoles (5-methoxy-1-phenyl-1*H*-tetrazole (5MPT) and 5-ethoxy-1-phenyl-1*H*-tetrazole (5EPT)) are presented. The choice of these compounds was based on two criteria required for having a relatively simple photochemistry: reduced number of stable conformations and inexistence of labile hydrogen atoms directly bound to the tetrazole ring or in the tetrazole substituents. This way, the photochemistry of 5MPT and 5EPT could be expected to be simpler than that observed for other tetrazoles of superior structural complexity,[10-14] and its study appeared potentially useful for allowing improvement of the knowledge on the photochemistry of this class of compounds.

Among the compounds investigated in our laboratories and discussed now in this Chapter, 5-methoxy-1-phenyl-1*H*-tetrazole (5MPT) was found to exhibit the less complex photochemistry.[10] According to the calculations (DFT(B3LYP)/6-311++G(d,p)), only one double degenerated-by-symmetry minimum exists in the ground-state potential energy profile of the compound. In this structure, the dihedral angle between the two rings, phenyl and tetrazole, is *ca.* 30°, whereas the methoxy group stays nearly in the plane of the tetrazole ring. In consonance with the theoretical predictions, only one molecular species was experimentally observed in the as-deposited argon matrices. Theoretical calculations were also used to help in assignment of the experimental spectrum of the compound, the calculated spectrum showing a very good agreement with the experimental data. *In situ* UV-irradiation ($\lambda > 235$ nm) of the matrix-isolated 5MPT induced unimolecular decomposition of the compound, which led mainly to production of methylcyanate and phenylazide, this latter further reacting to yield, as final product, 1-aza-1,2,4,6-cycloheptatetraene. 3-Methoxy-1-phenyl-1*H*-

diazirene was also observed experimentally as minor product, resulting from direct elimination of molecular nitrogen from 5MPT.

A similar study was carried out for 5-ethoxy-1-phenyl-1*H*-tetrazole (5EPT), combining matrix isolation FT-IR spectroscopy and theoretical calculations (DFT(B3LYP)/6-311++G(d,p)). Results of this investigation will be presented in Section 3.1.3. of this Chapter. Calculations show three minima, very close in energy and separated by low-energy barriers (less than 4 kJ mol^{-1}), in the ground-state potential energy profile of the molecule. The method of matrix isolation enabled the reduction of the number of populated conformational states in the experiment at low temperature due to the effect known as conformational cooling. As a result, the spectrum of the as-deposited matrix of 5EPT closely matches that of the most stable conformer predicted theoretically, pointing to the existence of only this conformer in the low-temperature matrices. In this structure, the dihedral angle between the two rings, phenyl and tetrazole, is *ca.* 30°, whereas the ethyl group stays nearly in the plane of the tetrazole ring and is as far as possible from the phenyl group. Similarly to the observed for 5MPT, UV-irradiation ($\lambda > 235$ nm) of the matrix-isolated 5EPT induced unimolecular decomposition of the compound. Ethylcyanate and phenylazide were identified as the main primary photoproducts, while 3-ethoxy-1-phenyl-1*H*-diazirene was observed as minor primary photoproduct. The two anti-aromatic diazirenes observed during the photodecomposition of 5MPT and 5EPT have not been described before and were characterized by infrared spectroscopy for the first time.

3.1.2. Infrared Spectrum and UV-induced Photochemistry of Matrix-isolated 5-Methoxy-1-phenyl-1*H*-tetrazole

- DFT structural calculations: molecular geometry

The optimized geometry of 5MPT, obtained at the DFT(B3LYP)/6-311++G(d,p) level of theory, is provided in Table S1 (Appendix B) and shown graphically in Figure 1.

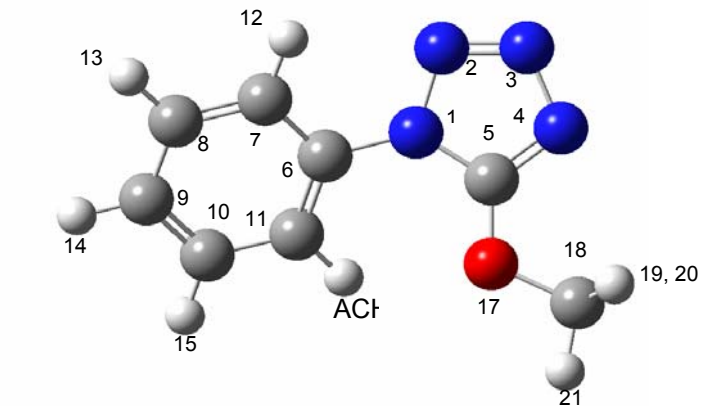

Figure 1. B3LYP/6-311++G(d,p) optimized geometry of 5-methoxy-1-phenyl-1*H*-tetrazole with atom numbering. Calculated energy (with zero point vibrational correction) and dipole moment are -1585361.34 kJ mol^{-1} and 5.2 debye. The $C_7C_6N_1C_5$ and $N_1C_5O_{17}C_{18}$ dihedral angles are predicted as being 151.3 and -177.0 degrees, respectively.

5-Methoxy-1-phenyl-1*H*-tetrazole has two rotational axes (–$C_{(6)}$–$N_{(1)}$– and –O–CH_3) that could in principle give rise to different conformers. However, only one minimum (doubly degenerated by symmetry) was located in the potential energy surface of the molecule. In the minimum energy structure, the molecule adopts a geometry in which the methyl group is as far as possible from the phenyl group ($N_{(1)}$–$C_{(5)}$–$O_{(17)}$–$C_{(18)}$ dihedral angle ~180° degrees) and the inter-ring twisting angle is *ca.* 30°.

The inter-ring angle is determined by the balance between three main factors: *i)* conjugation of the π electron systems of both rings, which favours their coplanarity; *ii)* steric repulsion between the substituents on the tetrazole ring, which favours a non-planar geometry; and *iii)* intramolecular H-bond-like interaction between the *ortho*-hydrogen atoms of the phenyl ring and $O_{(17)}$ or $N_{(2)}$ atoms ($H_{(12)}\ldots N_{(2)}$ and $H_{(16)}\ldots O_{(17)}$ interactions can be expected to favour coplanar and non-coplanar arrangements of the two rings, respectively). In view of the accumulated data on several molecules with two rings connected by a single bond (*e.g.,* 2-phenylpyridine, 2-phenylimidazole, 1-methyl-2-phenylimidazole, 4,6-dichloro-2-methylthio-5-phenylpyrimidine and several phenyl-substituted members of the tetrazole family[6,16-27]) among those three effects, the second appears to be the dominant one. Indeed, it has been demonstrated that the size of the sterically interacting substituents in the two rings is determinant on the relative orientation of the rings.[6,16-27] This effect is clearly observed, for example, when comparing 5-chloro-1-phenyl-tetrazole[6] with 5MPT. 5-Chloro-1-phenyl-tetrazole has larger interacting substituents and displays a larger inter-ring twisting angle (54.2° versus 28.7° in 5MPT, at the DFT(B3LYP)/6-311++G(d,p) level of theory). On the other hand, the inter-ring dihedral angle in 1-phenyl-tetrazole was found to be 12.8° in the crystalline phase,[24] *i.e.* smaller than in both 5MPT and 5-chloro-1-phenyl-tetrazole.

Note that the effect of the intramolecular H-bond-like interactions between the *ortho*-hydrogen atoms of the phenyl ring and O or N atoms was found to be relevant in 1-phenyl-tetrazolone, where both interactions tend to favour the coplanarity between the two rings.[10] In that molecule, the two rings were indeed found to be coplanar (inter-ring twisting angle: 0°; $H_{(16)}...O_{(17)}$ distance: 225.9 pm[19]). On the other hand, in both 1-phenyl-tetrazolone and 5MPT, conjugation of the π electron systems of phenyl and tetrazole rings does not seem to be very important, considering the estimated values for

the C–N inter-ring distance (142.6 and 142.4 pm, respectively), which can be compared with those found for alkylamines (essentially pure C–N single bond: within the 145–147 pm range [28]) and, for instance, methylenimine (H_2C=NH, double bond: 127.3 pm[29]). In simple diazines (pyrazine, pyrimidine and pyridazine), where the CN bond lengths have a bond order of *ca.* 1.5 – conjugated system – the bond lengths are *ca.* 133.5 pm,[30-32] *i.e.*, considerably shorter than the C–N inter-ring distance in 5MPT.

- Infrared spectrum of the matrix isolated compound (as-deposited matrix)

5MPT minimum energy structure belongs to the C_1 symmetry point group. It has 57 fundamental vibrations, all predicted to be active in the infrared. Figure 2 displays the spectrum of the as-deposited compound (nozzle temperature: 323 K). The matrix-isolated monomer of 5MPT gives rise to an IR spectrum that fits nicely the calculated spectrum [DFT(B3LYP)/6-311++G(d,p)], which is also shown in Figure 2, for comparison. Table 1 presents the proposed band-assignments. The definition of the internal coordinates used in this study to perform the normal coordinates analysis is given in Table S2 (Appendix B), while Table S3 (Appendix B) shows the full details of the calculated spectra, including normal mode characterization in terms of the potential energy distribution (PED).

In practical terms, the IR spectrum of 5MPT can be considered as being basically constituted by two groups of bands: one associated with the vibrational modes of the phenyl group and the other with the tetrazole ring.

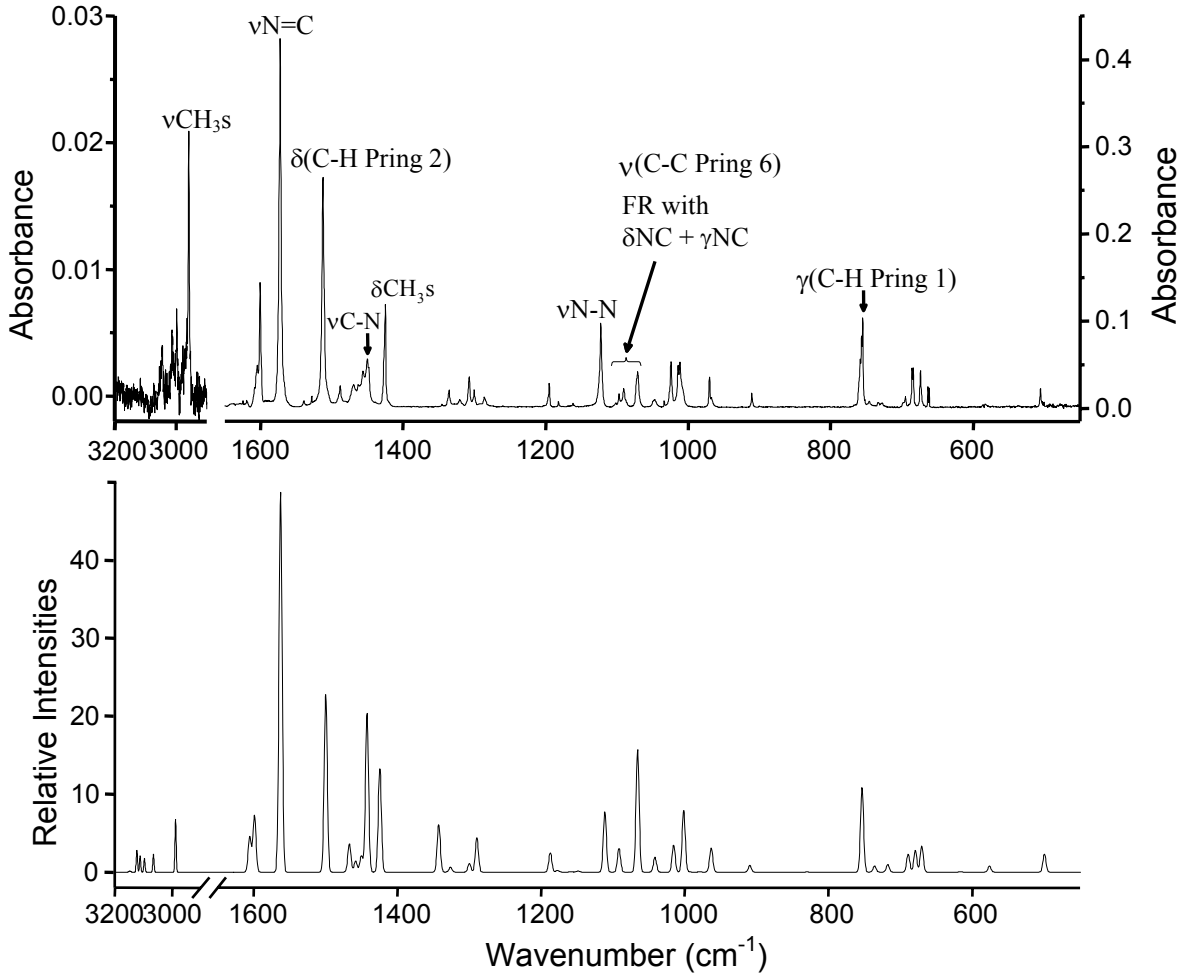

Figure 2. Infrared spectra of 5-methoxy-1-phenyl-1*H*-tetrazole. (*Top*) isolated in an argon matrix (conditions during deposition: substrate temperature= 9 K; nozzle temperature= 323 K); assignments for the most intense bands are provided (FR= Fermi resonance). (*Bottom*) B3LYP/6-311++G(d,p) calculated spectrum for the minimum energy conformation. Calculated spectra were simulated using Gaussian functions centered at the calculated (scaled 0.978) frequency and with bandwidth at half height equal to 5 cm^{-1}.

The bands corresponding to the first group show very slight differences among different 1-phenyl-tetrazole compounds, appearing at nearly the same frequencies in 1-phenyl-tetrazole,[6] 5-chloro-1-phenyl-tetrazole[6] and 1-phenyl-tetrazolone,[10] for example. This means that a second substituent on the tetrazole ring does not have a strong influence on the phenyl group, a result that is also in consonance with a small conjugation of the π electron systems of phenyl and tetrazole rings in 5MPT (also in agreement with these results is the fact that the optimized structures of the various 1-phenyl-tetrazole compounds already studied[6,10] do not show any substantial differences

in the geometry of the phenyl group). Contrary to what is observed for the phenyl vibrations, and as could be expected, the tetrazole ring vibrations are strongly affected by the substituent in the 5-position and differ considerably among different compounds.

Among the most intense bands in the 5MPT spectrum, the doublet at 1512.5/1510.5 cm^{-1} (δC–H P-ring 2), multiplet in the 1090-1070 cm^{-1} region (νC–C P-ring 6) and triplet at 758.5/756.5/754.9 cm^{-1} (γC–H P-ring 1) belong to the phenyl moiety (see Figure 2 and Table 1). These modes occur at 1505.2, 1078.2/1074.3 and 754.6/747.9/746.2 cm^{-1}, respectively, for 1-phenyl-tetrazolone,[10] at 1506.8, 1077.3 and 760.8 cm^{-1} for 5-chloro-1-phenyl-tetrazole[6] and 1511.8, 1089.5/1085.4 and 756.2 cm^{-1} for 1-phenyl-tetrazole.[6]

All the remaining most intense bands in the IR spectrum of 5MPT are associated with modes originated in the tetrazole ring or methoxy group and correspond to νN=C, νC–N, δCH_3 symmetric, νN–N and νO–C vibrational modes (see Figure 2 and Table 1). The νN=C vibrational mode gives rise to the most intense band of the spectrum and occurs as a site split doublet at 1572.3 and 1571.3 cm^{-1}. It represents *ca.* the fifth part of the total intensity of the spectrum (18.4% of the experimental spectrum and 21.8% of the calculated spectrum). In 1-phenyl-tetrazole and 5-chloro-1-phenyl-tetrazole,[6] the equivalent vibrations absorb at 1474.6/1471.4 and 1435.2/1429.5 cm^{-1}, respectively, thus *ca.* 100 cm^{-1} below the observed frequency for 5MPT. However, the $N_{(4)}=C_{(5)}$ bond lengths are similar in all three compounds.

Table 1. Observed frequencies (cm^{-1}) for 5-methoxy-1-phenyl-1*H*-tetrazole in an argon matrix. DFT(B3LYP)/6-311++G(d,p) calculated frequencies and intensities (km mol^{-1}) are given for comparison.[a]

Approximate Description	Calculated frequency	Intensity	Observed Frequency Ar (9 K)	I
ν(C–H P-ring 1)	3148.5	0.7	3117.0	w
ν(C–H P-ring 2)	3144.9	0.3	n.o.	
ν(C–H P-ring 3)	3123.0	14.8	3094.6	w
ν(C–H P-ring 4)	3111.7	10.9	3082.4	w
ν(C–H P-ring 5)	3101.5	0.0	n.o.	
νCH_3 as'	3096.5	9.3	3072.2	w
νCH_3 as''	3064.8	12.2	3045.8	w
2x δ(C–H ring 2)			3012.8	w
νN=C + νC–N			2997.7	w
νCH_3 s	2988.1	36.1	2958.8	m
ν(C–C P–ring 2)	1605.4	24.4	1604.6	m
ν(C–C P–ring 4)	1598.7	38.8	1600.5	m
νN=C	1562.4	259.5	1572.3/1571.3	S/sh
ν(C–C P–ring 1) + γNC			1539.2	w
δ(C–H P–ring 2)	1499.6	121.5	1512.5/1510.5	S/sh
γ(C–H P–ring 1) + νC-O			1488.5	w
δCH_3 as'	1466.8	19.4	1469.6	m
δ(C–H P–ring 3)	1458.0	7.5	1462.5	w
δCH_3 as''	1450.0	10.9	1456.3	m
νC–N	1442.1	108.4	1450.1/1448.0	m/m
δCH_3 s	1424.3	70.9	1426.1/1424.8	sh/m
2x τ(T–ring 1)			1345.6	w
νN=N	1342.4	32.4	1335.4	w
δ(C-H P–ring 1)	1326.1	3.4	1320.5	w
ν(C-C P–ring 3)	1299.7	5.8	1307.1	w
νN-C [FR with δ(T-ring 1)+δ(P-ring 2)]	1289.2	23.4	1300.2/1298.7/1286.2/1284.0	w/sh/w/sh
2x δ(P–ring 2)			1248.1	w
γCH_3'	1187.2	13.1	1195.1	m
δ(C–H P-ring 4)	1177.2	1.2	1182.1	w
δ(C–H P-ring 5)	1158.7	0.2	1169.1	w
γCH_3''	1148.6	0.7	1161.6	w
νN–N	1111.3	41.3	1122.7	m
δ(T–ring 2)	1091.5	16.1	1101.3/1096.9	w/w
ν(C–C P-ring 6)[FR with δNC + γNC]	1065.7	84.0	1090.4/1087.5/1072.9/1070.9	w/sh/sh/m
ν(C–C P-ring 5)	1041.6	10.0	1046.8	w
ν(C–C P-ring 1)	1015.6	18.5	1024.1	m
νO–C [FR with 2x γNC]	1001.5	42.1	1014.2/1011.5	m/m
δ(P–ring 1)	994.8	0.3	n.o.	
γ(C–H P-ring 5)	979.3	0.1	n.o.	
τ(P–ring 3)	965.0	2.4	985.2	w
νN–N'	963.1	14.6	969.9/967.2	m/m
γ(C–H P-ring 3)	909.5	4.4	910.6/909.2	w/sh
γ(C–H P-ring 2)	830.3	0.1	n.o.	
γ(C–H P-ring 1)[FR with 2x γCO]	753.4	57.8	758.5/756.5/754.9	m/m/m
νC–O	736.2	4.1	745.7	w
τ(T–ring 2)	717.7	5.1	733.5/727.9	w
τ(T–ring 1)	689.3	12.4	697.5/695.0	w/w
τ(P-ring 1)[FR with 2x δ(P-ring 3)]	679.4	14.8	685.9/684.0	w/w
δ(T-ring 1)	670.4	17.9	674.0	w
δ(P-ring 2)	616.5	0.2	623.7	w
δNC	576.2	3.9	583.0	w
γNC	499.6	12.2	505.6	w
γ(C-H P-ring 4)	405.5	0.2	n.o.	

[a] I, intensity; ν, bond stretching, δ, bending, γ, rocking, τ, torsion, s, symmetric, as, antisymmetric; FR, Fermi resonance. See Table S2 for definition of internal coordinates. S, strong; m, medium; w, weak, sh, shoulder; n.o., not observed; calculated frequencies and intensities for modes below 400 cm^{-1} (region not experimentally investigated) are given in Table S3. T-ring, tetrazole ring; P-ring, phenyl ring.

Thus, the difference in observed frequencies reflects essentially the vibrational coupling, which is substantially different in 5MPT when compared with the other two compounds, and should not reflect any substantially different electronic characteristics (such as bond order) of the $N_{(4)}=C_{(5)}$ bond in the three compounds. Indeed, according to the calculations, in 5MPT the contribution of the νC–O coordinate of the methoxy substituent to this mode is very important (35.5%; see Table S2 (Appendix B)), what by itself changes pronouncedly the nature of the vibration when compared with those of 1-phenyl-tetrazole and 5-chloro-1-phenyl-tetrazole.[6]

νC–N (associated with the $C_{(5)}–N_{(1)}$ bond) is observed at 1450.1/1448.0 cm^{-1} and is the third most intense band in the spectrum (see Table 1 and Figure 2). It is quite coupled with the νN=C coordinate (see Table S2 (Appendix B)), what justifies its relatively high frequency when compared, for instance, with that corresponding to the stretching mode of the $N_{(1)}–C_{(6)}$ inter-ring distance (observed as a multiplet in the 1300–1284 cm^{-1} region; Table 1). νN–N (associated with the $N_{(3)}–N_{(4)}$ bond) is observed at 1122.7 cm^{-1} and does also correspond to a considerably delocalized mode, whereas the δCH_3 symmetric vibration is observed as a site split doublet at 1426.1/1424.8 cm^{-1}, being, as expected, a well localized vibration [see Table S2 (Appendix B)]. Finally, νO–C is the last vibration among the most intense bands of the tetrazole ring and methoxy substituent mentioned above. It is a relatively well-localized vibration and absorbs (1014.2/1011.5 cm^{-1}) within the characteristic frequency range for this mode in methyl esters and methyl ethers (around 1050-950 cm^{-1}).[33]

Taking into consideration the good agreement between the experimental and calculated spectra (see Figure 2), the assignment of the weaker bands in the observed spectrum could also be made in a straightforward way. A few weak bands that could not

be assigned to fundamentals were also identified in the spectrum and tentatively ascribed to overtones or combination bands, as shown in Table 1.

- UV- irradiation experiments ($\lambda > 235$ nm)

Upon broadband UV-irradiation ($\lambda > 235$ nm) of matrix-isolated monomeric 5MPT the spectrum of the compound lost intensity, while new bands developed. The most prominent features of the photoproducts were observed in the 2300-1700 cm^{-1} spectral range, though other features could also be observed in the low frequency spectral region, including a relatively intense feature around 1380 cm^{-1} (Figure 3). The complete list of bands due to the products of photolysis of 5MPT is presented in Table 2. The proposed reaction pathways are schematically shown in Figure 4.

As it could be expected, comparatively to other previously studied tetrazoles[6-10] the observed photochemistry of 5MPT was considerably simpler. Essentially, two reaction pathways could be identified: *(1)* cleavage of the tetrazole ring through the $C_{(5)}–N_{(1)}$ and $N_{(3)}–N_{(4)}$ bonds, with production of phenylazide and methylcyanate as primary photoproducts (phenylazide can then undergo further reactions to give 1-aza-1,2,4,6-cycloheptatetraene – ACHT) and *(2)* molecular nitrogen elimination, leading to formation of antiaromatic 3-methoxy-1-phenyl-1*H*-diazirene (MPD). The first process is clearly the preferred reaction channel, as it can be noticed by comparing the relative intensities of the mark bands due to the different photoproducts, appearing in the 2300-1700 cm^{-1} spectral range.

Table 2. Experimental and calculated [B3LYP/6-311++G(d,p); scaled by 0.978] vibrational frequencies and calculated IR intensities for the observed photoproducts of 5-methoxy-1-phenyl-1*H*-tetrazole isolated in solid argon.[a]

Approximate description[b]	Symmetry	Calculated		Observed frequency (cm^{-1})	Literature frequency (cm^{-1})
		Frequency (cm^{-1})	Intensity (km mol^{-1})		
Methylcyanate	C_s				(gas phase) [32]
νOCN as.	A"	2300.9	208.6	2265.7[c]/2255.4	2263
δCH_3 as.'	A'	1461.4	16.4	1462.1	1470
δCH_3 as. "	A"	1455.1	12.2	1453.4	1462
γ CH_3'	A'	1200.1	62.1	1215.3	1213
νOCN s.	A'	1110.9	104.2	1107.2	1112
νC–O	A'	864.1	39.3	874.0	893
Phenylazide	C_s				(N_2 matrix) [34]
νN=N=N as.	A'	2191.4	843.5	2174.6/2164.7 2134.3/2129.6	2165/2157/2137/2128[c] 2112/2102/2087
ν(C–C ring 2)	A'	1600.5	59.2	1618.4	1598
ν(C–C ring 4)	A'	1585.3	6.4	1581.3	1589/1585
δ(C–H ring 2)	A'	1487.7	86.3	1502.8	1496/1491
νN=N=Ns.	A'	1336.4	151.2	1382.7/1380.8	1398
δ(C–H ring 1)	A'	1325.0	29.8	1316.7	1337
ν(C–C ring 3)	A'	1296.8	18.2	1300.8/1295.7	1305/1298
δ(C–H ring 4)	A'	1174.6	2.4	1174.4 (?)	1176
νN C	A'	1128.9	18.3	~1125[d]	1136/1131
ν(C–C ring 5)	A'	1022.0	4.4	1039.0	1026
γ (C–H ring 3)	A"	887.7	5.2	908.4	896
δCNN	A'	805.5	5.3	813.3	810
γ (C–H ring 1)	A"	744.9	68.7	740.4	751
τ(ring 1)	A"	675.2	23.2	662.1	687
δNNN	A'	666.9	25.1	655.3	670
ACHT	C_1				(Ar matrix) [33]
νC =C=N as.		1913.1	202.2	1891.5	1895
δ(C–H 1)		1201.8	3.9	1215.3[e]	
δ(C–H 2)		1110.9	15.2	1107.2[e]	1111
νN–C		979.7	25.6	986.7	980
γ (C–H 1)		951.4	3.0	940.0	940
γ (C–H 2)		945.7	4.5	935.4	
γ (C–H 3)		754.3	62.3	~754[d]	748
δCCN		685.0	45.5	689.7	683
τ(ring 1)		663.8	28.2	652.4	658/650
γ CCN		595.5	10.9	587.5	580
MPD	C_1				
νC=N		1768.7	431.3	1738.5/1733.0/1731.0	
δCH_3 as.'		1465.7	17.7	1471.2	
δCH_3 as."		1454.8	14.1	1462.1[e]	
δ(C–H ring 2)		1449.0	7.8	1458.1	
νC–N		1354.8	111.8	1402.3	
δ(C–H ring 1)		1297.0	6.8	1271.1	
νN–C		1194.3	72.5	1215.3[e]	
γ CH_3'		1187.4	13.7		
δ(C–H ring 4)		1159.4	18.3	1155.0	
δ(C–H ring 5)		1154.0	7.6		
νO–C(H_3)		1028.5	133.4	1057.9	
ν(C–C ring 5)		1018.3	47.2	1039.0[f]	
γ (C–H ring 3)		908.1	2.8	914.8 (?)	

Table 2. (Continued)[a]

νC–O	867.6	18.0	874.0[e]
γ (NN(C)O)[g]	804.6	9.4	801.1
γ (C–H ring 1)	763.6	36.1	~754[d]
τ(ring 1)	675.0	36.5	~685[d]

[a] Complete calculated spectra are presented in Tables S4–S7 (Appendix B).
[b] ν, stretching; δ, bending; γ, rocking; τ, torsion; ring modes were given the names in consonance with those used for 5MPT.
[c] Shoulder.
[d] Overlapped with a band of the reactant (5MPT).
[e] Overlapped with a band of methylcyanate.
[f] Overlapped with a band of phenylazide.
[g] C out of the N–N–(C)–O plane bending vibration.

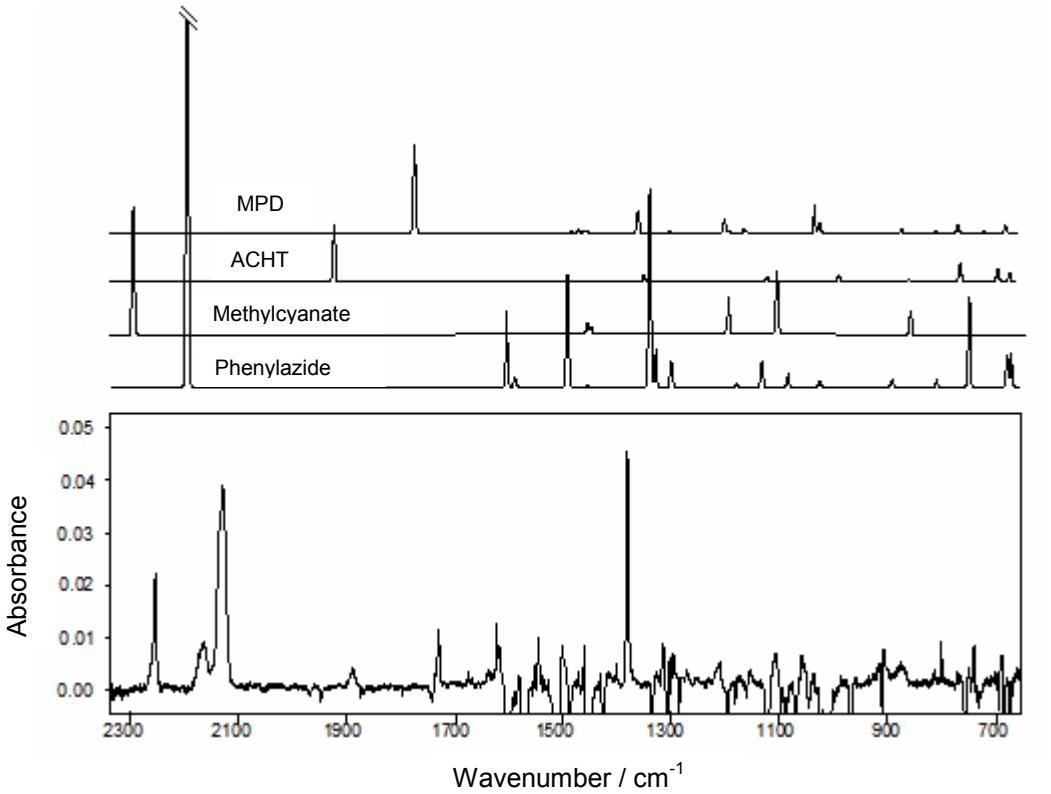

Figure 3. (*Bottom*) Changes in infrared spectrum of 5MPT trapped in an argon matrix induced by UV (λ>235 nm) irradiation (spectrum of UV-irradiated (80 min) sample minus spectrum of freshly deposited matrix). (*Upper frames*) B3LYP/6-311++G(d,p) calculated spectra of the observed photoproducts. In the theoretical spectra, intensities were scaled by different factors, in order to better simulate the experimental spectrum presented in the figure. The complete calculated spectra are provided in Tables S4–S7 (Appendix B).

Both observed photoprocesses imply cleavage of the $N_{(3)}$–$N_{(4)}$ bond. The first one also implies disruption of the $C_{(5)}$–$N_{(1)}$ bond, while the second one requires cleavage of the $N_{(1)}$–$N_{(2)}$ bond. According to the calculations, these are the three longest bonds in the tetrazole ring [with calculated lengths longer than 135.5 pm; see Table S1 (Appendix B)].

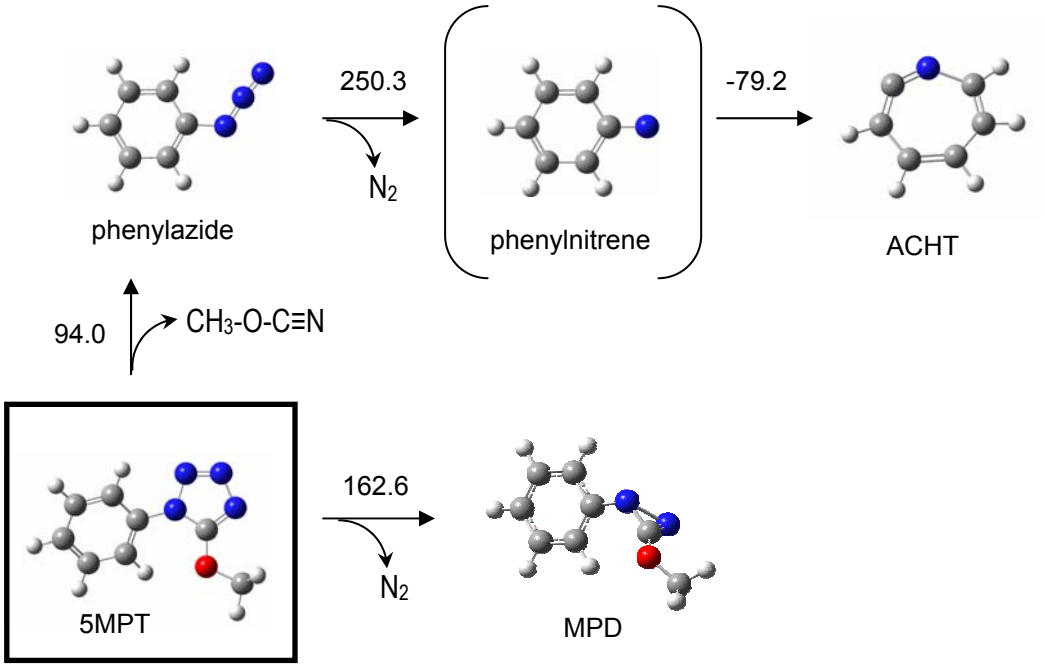

Figure 4. Proposed pathways resulting from irradiation of 5-methoxy-1-phenyl-1*H*-tetrazole in an argon matrix through the outer KBr window of the cryostat (λ > 235 nm). Reaction energies (with zero point corrections) are in kJ mol^{-1}.

The $N_{(2)}$=$N_{(3)}$ and $C_{(5)}$=$N_{(4)}$ bonds are considerably shorter (128.0 and 131.3 pm, respectively, as calculated at the DFT(B3LYP)/6-311++G(d,p) level of theory). Hence, the bonds that are directly involved in the reactions correspond to the weaker bonds. Moreover, for this molecule, both the HOMO and the LUMO are of π-character (Figure 5). According to the calculations, the vertical π*←π excitation corresponding to a single excitation from the HOMO to the LUMO (roughly estimated from the LUMO-HOMO energy difference) has a wavelength of *ca.* 220 nm, which doubtlessly indicates that this corresponds to the reactive excitation. Very interestingly, contrarily to the HOMO orbital, which has a bonding character on the $C_{(5)}$–$N_{(1)}$ bond, the LUMO is anti-bonding on this bond, thus explaining why it is so easy to break this bond upon photochemical excitation at λ > 235 nm. Note that the LUMO orbital does also have an anti-bonding character on the $N_{(1)}$–$N_{(2)}$ bond, which is cleaved in the alternative reaction path instead of $C_{(5)}$–$N_{(1)}$ (see Figure 5). The preference for the reaction path leading to phenylazide

and methylcyanate, when compared with that leading to molecular nitrogen plus MPD, is also in consonance with the reaction energies (94.0 and 162.6 kJ mol^{-1}, respectively; see Figure 4), which clearly favour the first process relatively to the second one.

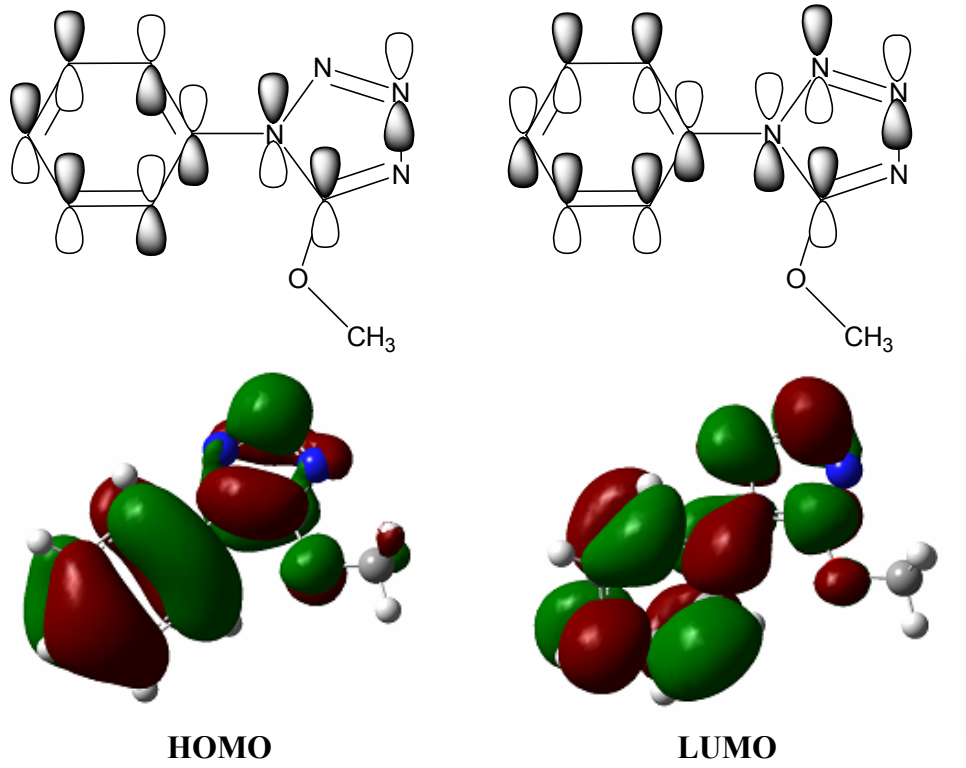

Figure 5. (*Top*) Schematic representation of the HOMO and LUMO of 5MPT. (*Bottom*) HOMO and LUMO of 5MPT, calculated at the DFT(B3LYP)/6-311++G(d,p) level of theory. The isosurface corresponds to the electronic density of 0.02 *e*.

All strong and medium intensity bands predicted for the two major products formed in *Pathway 1* (phenylazide and methylcyanate) could be observed in the spectra of the irradiated matrix (see Figure 3 and Table 2). Methylcyanate is a quite unstable compound under normal experimental conditions and in particular in solid phase, isomerizing quickly to its more stable isomer methylisocyanate[34-37] [the DFT(B3LYP)/6-311++G(d,p) calculated energy of methylisocyanate is 127.5 kJ mol^{-1} lower than that of methylcyanate]. Its synthesis was first reported in 1965, by two different groups,[34,35] although a pure sample could not be obtained for spectroscopic

investigation because of the instability of the molecule. This was only achieved much later, when Pasinszki and Westwood[36] reported the mid-infrared spectrum of gaseous methylcyanate. All vibrations of methylcyanate absorbing above 650 cm^{-1}, except the δCH_3 symmetric bending mode [calculated intensity: 0.9 km mol^{-1}; see Table S4 (Appendix B)], could be identified in the registered spectrum and duly assigned.[36] In the present study, all bands reported for the gas phase could also be observed in the spectra of the irradiated matrix (Table 2), with the only exception of the very weak band due to γCH_3" mode [appearing at 1199 cm^{-1} in the gas phase;[36] calculated intensity: 0.6 km mol^{-1}; Table S4 (Appendix B)], unequivocally testifying for the presence of this species in the matrix. Very interestingly, no evidence of isomerization of methylcyanate to methylisocyanate was found, indicating that under the experimental conditions used, methylcyanate is stable in relation to the isomerization to the isocyanate.

Phenylazide is produced in *Pathway 1* together with methylcyanate (Figure 4). This compound has been previously isolated and irradiated in both argon and nitrogen matrices, and production of 1-aza-1,2,4,6-cycloheptatetraene (ACHT) unequivocally demonstrated.[10,38-40] The vibrational spectra of matrix-isolated phenylazide and of ACHT are then well known and their identification could be made here without any difficulty (see Table 2).

As found in a previous study on 1-phenyl-tetrazolone,[10] under the experimental conditions used, phenylazide reacts with relatively low efficiency, in particular when compared to the reactions undergone by the tetrazole compounds. The intermediate for this reaction is, with all probability, singlet phenylnitrene, which has been found to easily undergo ring expansion to ACHT (the calculated ground state energies for these two species favour the latter compound by *ca.* 80 kJ mol^{-1} – see Figure 4). Characteristic bands of ACHT[10,41,42] could be clearly identified in the spectra of the

irradiated matrix. Particularly noticeable is the intense band-mark associated with the antisymmetric stretching of the ketenimine moiety (νC=C=N *as*.) of ACHT, observed at 1891.5 cm^{-1}, (Figure 3). Other bands previously described by Chapman and Le Roux as well as by Huisgen *et al*.[38,42] as fingerprints of this compound, could also be clearly identified in the spectra (Table 2). Note also that, as was previously found for UV-irradiated 1-phenyl-tetrazolone monomer isolated in argon,[10] triplet phenylnitrene (reported to be present in low temperature matrices as a result of direct photolysis of isolated phenylazide[40]) was not observed in the present study, even when irradiation was undertaken using different wavelength cut-off filters (*e.g.*, 285, 337, 375 and 417 nm). Like previously suggested,[10] the absence of observation of triplet phenylnitrene may result from the fact that phenylazide is produced together with other species and might interact in the matrix cage, eventually making inaccessible the pathway which would lead to formation of the triplet nitrene.

Pathway 2 involves the loss of molecular nitrogen to produce 3-methoxy-1-phenyl-1*H*-diazirene (MPD; Figure 4), which was now observed for the first time. The ejection of molecular nitrogen after irradiation of tetrazole compounds to give diazirenes has already been described.[6,10] Diazirenes can be easily identified because their most intense band [νC=N; see Tables 2 and S6 (Appendix B)] occurs in a "clean" region of the spectrum (1850-1720 cm^{-1}) and can be considered as fingerprint of this family of compounds. Only one conformer was located on the potential energy surface of MPD. Hence, the structure observed in the feature assigned to this compound at around 1735 cm^{-1} should be attributed to matrix site splitting. On the whole, MPD has 51 infrared vibrations. However, in the studied region (between 2300 and *ca.* 600 cm^{-1}) the calculations predict only 17 modes with intensities larger than 6 km mol^{-1} [see

Table S6 (Appendix B)]. From them, 16 could be assigned to bands observed in the spectra of the irradiated matrix (Table 2).

▪ Conclusions

In this work, monomeric 5-methoxy-1-phenyl-1*H*-tetrazole (5MPT) was isolated in solid argon and its infrared spectrum fully assigned. *In situ* UV-irradiation ($\lambda > 235$ nm) of the matrix led to the production of methylcyanate and phenylazide, in one reaction channel, and also of the antiaromatic 3-methoxy-1-phenyl-1*H*-diazirene (MPD), in the other. The primarily formed phenylazide is partially converted into 1-aza-1,2,4,6-cycloheptatetraene (ACHT), with all probability involving singlet phenylnitrene as intermediate. The identification of all the photoproducts as well as the interpretation of the spectrum of the isolated 5MPT were supported by extensive DFT calculations and, whenever available**,** by previously reported data on these compounds as matrix isolated species or in the gaseous phase.[6,10,36-38]

The relatively simple photochemistry of 5MPT, when compared with previously studied tetrazoles,[5-10,39] was attributed to two main facts: *i)* it has only one stable conformation and; *ii)* it does not have labile hydrogen atoms directly bound to the tetrazole ring or in tetrazole substituents. This relative simplicity allowed attaining a high degree of certainty in the identification and characterization of the different photoproducts and shed light on important details of the photochemistry of tetrazoles.

3.1.3. Photochemistry and Vibrational Spectra of Matrix-isolated 5-Ethoxy-1-phenyl-1*H*-tetrazole

- DFT structural calculations: molecular geometry

The molecule of 5-ethoxy-1-phenyl-1*H*-tetrazole has three internal rotational degrees of freedom, defined about the $-C_{(6)}-N_{(1)}-$, $-O-C_{(5)}-$ and $-O-C_{(18)}-$ bonds, which may result in the existence of different conformers (Figure 6).

The dihedral angle around the $C_{(6)}-N_{(1)}$ bond defines the relative orientation of the phenyl and tetrazole rings. Calculations show that in all conformers these two rings have approximately planar geometries. However, they do not share the same plane. In all forms the inter-ring CNCC angle was predicted by the calculations to be *ca.* 30 degrees [see Table S8 (Appendix B)].

The conformers with the *cis* orientation of the $N_{(1)}-C_{(5)}-O_{(17)}-C_{(18)}$ angle bring the ethyl and phenyl groups in a close spatial proximity and result in very high relative energies (*ca.* 84 and 79 kJ mol^{-1}, for planar and non-planar structures, respectively). Such conformers are not relevant from the experimental point of view and may be disregarded. The conformers with the *trans* orientation of the $N_{(1)}-C_{(5)}-O_{(17)}-C_{(18)}$ angle are energetically much more stable. They may differ in the orientation of the ethyl group relatively to the tetrazole ring, which is defined by the conformation around the $C_{(18)}-O_{(17)}$ bond (see Figure 6).

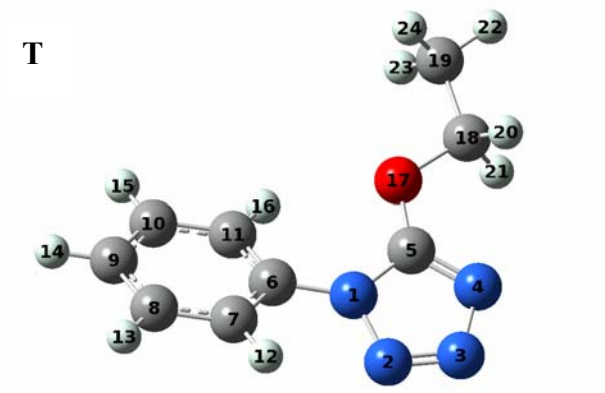

ΔE = 0.0 kJ mol^{-1}

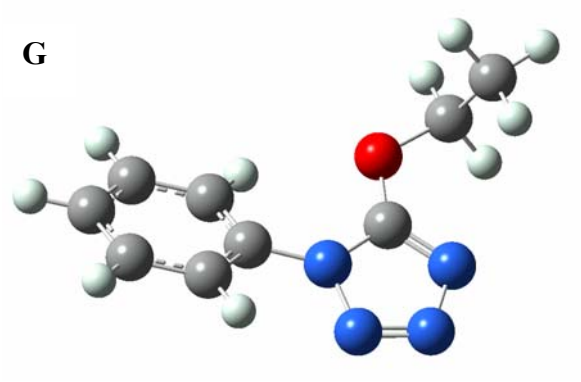

ΔE = 2.3 kJ mol^{-1}

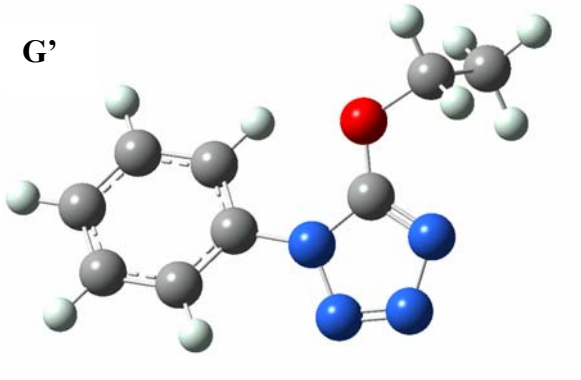

ΔE = 2.6 kJ mol^{-1}

Figure 6. Optimized structures for the 5-ethoxy-1-phenyl-1*H*-tetrazole conformers **T, G** and **G'** (with atom numbering). Relative energies calculated at the B3LYP/6-311++G(d,p) level of theory are also given (with zero point correction). Absolute calculated energy of conformer **T** is equal to −1689043.2 kJ mol^{-1}.

The potential energy profile for internal rotation around the $C_{(18)}$–$O_{(17)}$ bond in 5EPT is shown in Figure 7. This potential energy profile was calculated by incrementing the value of the $C_{(5)}$–$O_{(17)}$–$C_{(18)}$–$C_{(19)}$ dihedral angle in steps of 20 degrees and fully optimizing all other geometric parameters. This relaxed potential energy scan revealed the existence of three local minima (see Figure 7), with relative energies falling into the 0-3 kJ mol^{-1} range. The most stable structure exhibits the *trans* orientation of the ethyl group relatively to the tetrazole fragment, while the remaining conformers have the ethyl group in the ±*gauche* position relatively to the tetrazole ring. The energies of the latter forms (including zero point energy corrections) are 2.3 and 2.6 kJ mol^{-1} higher than that of the most stable form.

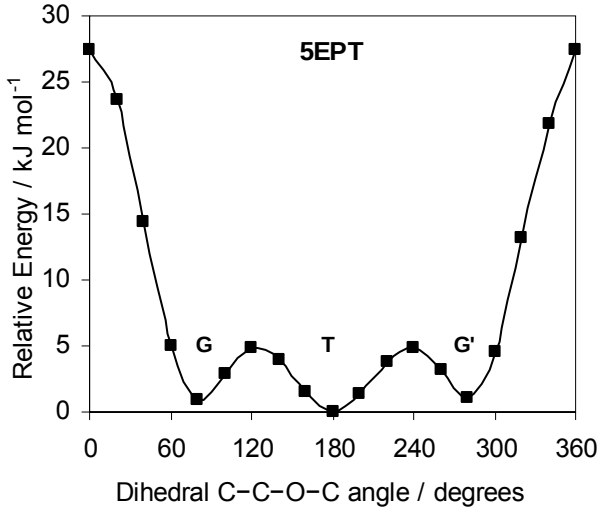

Figure 7. DFT(B3LYP)/6-311++G(d,p) calculated potential energy profile for internal rotation of the ethoxy group around the $C_{(18)}$–$O_{(17)}$ bond in 5-ethoxy-1-phenyl-1*H*-tetrazole. Minima denoted as **T**, **G** and **G'** correspond to the conformers with the same names in Figure 6. The energy of conformer **T** (the lowest-energy structure) is equal to −643.322495 hartree (without the ZPE contribution) and was chosen as the relative zero level.

It is logical to relate the names of different conformers with the values of the conformationally relevant dihedral angles. As was noted above, in all experimentally relevant conformers of 5EPT the values of two of these dihedral angles (CNCC and NCOC) are nearly equal and may be conveniently omitted from the conformers' names. In this work, the names of the relevant 5EPT conformers were then assigned according to the value of the COCC dihedral angle they exhibit: **T** (*trans*; most stable conformer), **G** (+*gauche*) and **G'** (−*gauche*), which are uniquely related with a COCC dihedral angle of *ca.* 180, +80 and −80 degrees, respectively. The optimized structures of the **T**, **G** and **G'** conformers of 5EPT, calculated at the DFT(B3LYP)/6-311++G(d,p) level of theory, are depicted in Figure 6. No other low energy local minima were found.

The calculated potential energy profile shown in Figure 7 revealed that the energy barriers separating forms **G** and **G'** from the most stable form **T** are very low, amounting to less than 4 kJ mol^{-1}. In conformational studies of matrix-isolated molecules, the knowledge of the barriers to intramolecular rotation is very important. It is well-known that the possibility of trapping a species in the matrix is related with the barriers to intramolecular rotation separating it from lower energy species.[43] If a barrier is low enough (a few kJ mol^{-1}), it can be surpassed even at low temperatures and the higher energy species will relax into the lower energy counterpart – the so-called conformational cooling will occur. Recently, a series of matrix isolation studies on the structure of conformationally flexible compounds was carried out in our laboratory in order to analyze the conformational cooling effect.[44-49] It was shown that intramolecular energy barriers lower than 5 kJ mol^{-1} are effectively surpassed at 10 K, already at the stage of the matrix deposition. Barriers of at least 10 kJ mol^{-1} are in general required to trap a given conformer in a matrix. Thus, based on this experience, one can also assume that the same phenomenon takes place in the case of 5EPT, resulting in relaxation of the

higher energy forms, **G** and **G'**, into the lowest energy conformer, **T**. The experiment confirmed this expectation: Figure 8 represents the spectrum of 5EPT isolated in an argon matrix at 12 K, which is in excellent agreement with the theoretically calculated spectrum of conformer **T**.

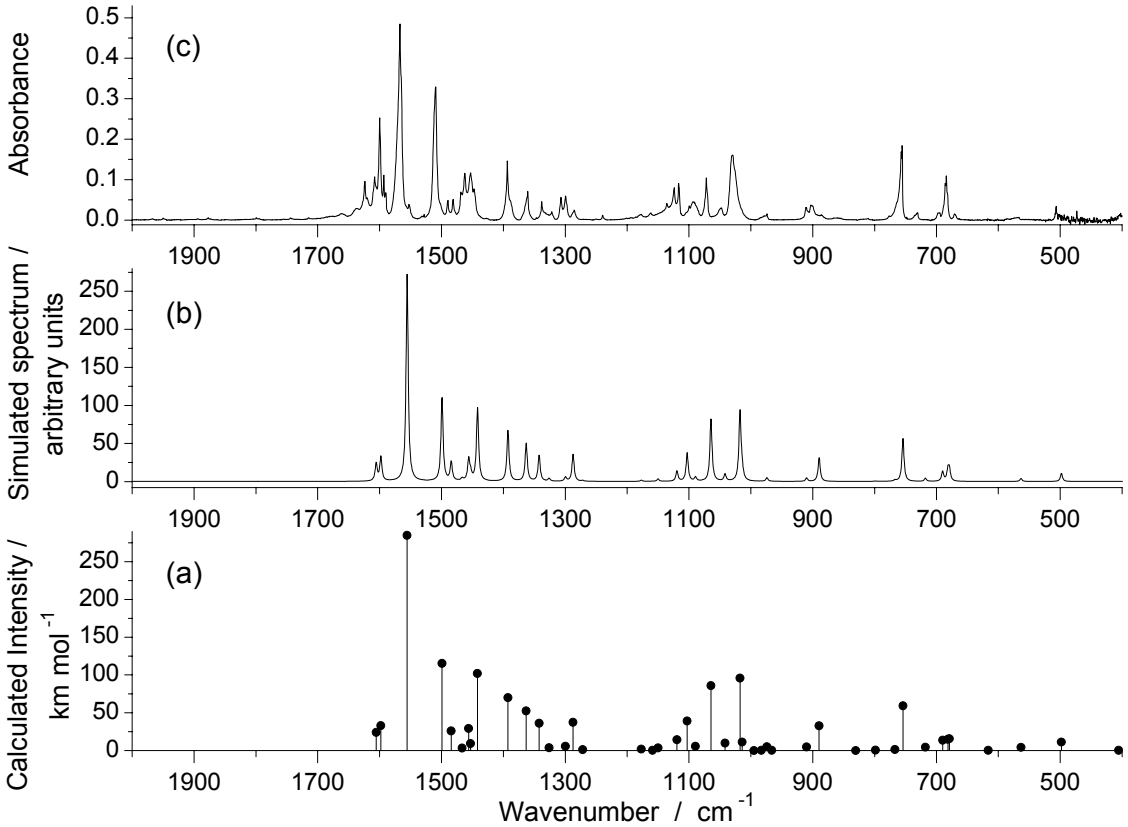

Figure 8. Infrared spectrum of 5EPT in the fingerprint region: **(a)** spectrum of conformer **T** calculated at the B3LYP/6-311++G(d,p) level of theory. Calculated wavenumbers were scaled by a factor of 0.978; **(b)** simulated spectrum of conformer **T**, created using Lorentzian functions centered at the calculated (scaled) frequencies [shown in Frame **(a)**] and with bandwidths-at-half-height equal to 4 cm^{-1}. Intensities in this spectrum were scaled arbitrarily; **(c)** experimental spectrum of monomeric 5EPT trapped in an argon matrix at 12 K.

The observed conformational cooling led to existence of 5EPT in the studied low temperature matrices exclusively as its most stable conformer **T**. This is a very fortunate situation, since the experimental spectra of 5EPT is not complicated by conformational effects, which in turn will facilitate the interpretation of the photochemical processes taking place in the matrix, once subjected to *in situ* UV irradiation ($\lambda > 235$ nm), that will be described in detail below.

Considering the minimum energy structure of 5EPT (conformer **T** in Figure 6), it can be easily verified that the molecule assumes a geometry in which the ethyl group stays almost in the plane of the tetrazole ring and is situated as far as possible from the phenyl group ($C_{(5)}$–$O_{(17)}$–$C_{(18)}$–$N_{(19)}$ dihedral angle ≈180°), with an inter-ring twisting angle of 30.4 degrees. The value of the inter-ring angle is largely determined by the balance between three factors: (i) steric repulsion between the substituents on the tetrazole ring, which favour a non-planar geometry; (ii) conjugation of the π electron systems of both rings, favouring their co-planarity; and (iii) intramolecular H-bond-like interaction between the *ortho*-hydrogen atoms of the phenyl ring and the negatively charged $O_{(17)}$ or $N_{(2)}$ atoms located in the tetrazole side of the molecule ($H_{(12)}\cdot\cdot\cdot N_{(2)}$ and $H_{(16)}\cdot\cdot\cdot O_{(17)}$ interactions can be expected to favour coplanar and non-coplanar arrangements of the two rings, respectively).

It has been verified that the first factor appears to be dominant for many molecules with two rings connected by a single bond.[6,10,20-27] For instance, it is known that the chlorine substituent in 5-chloro-1-phenyl-*1H*-tetrazole (5CPT) is responsible for the large inter-ring angle (54.2 degrees) observed for this tetrazole derivative.[7] Hence, the steric effect due to the presence of the chloro substituent at $C_{(5)}$ in the 5CPT molecule is clearly more important than the corresponding effect caused by the ethoxy group attached to the same position in 5EPT (inter-ring angle; 30.4 degrees). In addition, the inter-ring dihedral angle in 5-methoxy-1-pheny-1*H*-tetrazole was found to be 28.7 degrees,[10] *i.e.* smaller than in 5CPT and similar to that found for all low energy conformers of 5EPT (see Table S8), indicating that in the experimentally relevant conformers of these molecules (all exhibiting the *trans* arrangement around the $-C_{(5)}-O_{(17)}-$ bond) the orientation of the ethyl substituent does not influence the interaction between the two rings.

On the other hand, in 5EPT, like for 5MPT, the conjugation of the π electron systems of phenyl and tetrazole rings does not seem to be very important, considering the estimated values for the C–N inter-ring distance in these two molecules (142.5 and 142.4 pm, respectively), which are similar to those found in alkylamines (essentially pure C–N single bonds: within the 145-147 pm range)[28] and, substantially longer than those observed, for instance, in methylenimine (H_2C=NH, double bond: 127.3 pm)[29] or in simple diazines [pyrazine, pyrimidine and pyridazine, where the CN bond lengths have a bond order of *ca.* 1.5 (conjugated system) and the bond lengths are *ca.* 133.5 pm].[30-32]

- Infrared spectrum of the matrix-isolated compound (as-deposited matrix)

As mentioned before, the infrared spectrum of the matrix-isolated 5EPT is presented in Figure 8, together with the B3LYP/6-311++G(d,p) theoretical spectrum of conformer **T**. As was noted above, the agreement between the experimental and calculated spectra is very good, enabling the full assignment of the experimental bands. The assignments are provided in Table 3 [results of vibrational calculations for the three conformers of 5EPT, including the definition of the used internal coordinates, are provided in Tables S9-S12 (Appendix B)].

Table 3. Observed frequencies (cm^{-1}) for 5-ethoxy-1-phenyl-1*H*-tetrazole in an argon matrix. DFT(B3LYP)/6-311++G(d,p) calculated frequencies (cm^{-1}; scaled by 0.978) and intensities (km mol^{-1}) are given for comparison.[a]

Approximate Description	Calculated frequency	Intensity	Experimental frequency	Intensity
ν(C–H P-ring 1/2)	3149.9	0.7	3203.6	w
ν(C–H P-ring 1/2)	3144.6	0.3	3203.6	w
ν(C–H P-ring 3)	3123.2	15.1	3203.6	w
ν(C–H P-ring 4)	3111.6	11.1	3203.6	w
ν(C–H P-ring 5)	3101.7	0.0	3075.6	w
νCH_3 as''	3052.8	30.4	3075.6	w
νCH_3 as'	3039.4	21.5	3075.6	w
νCH_2 as	3028.3	0.1	3003.9	sh
νCH_2 s	2992.1	14.3	3000.8/29985.2	w/w
νCH_3 s	2973.0	12.1	2967.4/2955.3/ 2939.8	w/w/w
ν(C–C P-ring 2)	1605.5	24.0	1593.2	m
ν(C–C P-ring 4)	1598.0	33.0	1590.0	m
νC–O/νN=C	1555.5	284.9	1567.2/1565.2/ 1552.5	S/sh/w
δ(C–H P-ring 2)	1499.2	115.2	1509.5	S
δCH_2	1484.2	26.0	1489.6/1481.3	w/w
δCH_3 as'	1466.6	3.4	1468.7	m
ν(C–H P-ring 3)	1456.0	29.2	1462.3	m
δCH_3 as''	1452.8	9.0	1462.3	m
νC–N	1441.8	102.0	1453.0/1447.5	m/m
δCH_3 s	1392.6	69.9	1393.6/1388.5	S/sh
ωCH_2	1363.1	52.4	1363.9/1360.6	sh/m
νN=N	1342.2	35.9	1338.0	m
δ(C–H P-ring 1)	1326.1	3.9	1321.8	w
ν(C–C P-ring 3)	1299.6	5.6	1306.9	m
νN=C/νN–C	1287.3	37.4	1299.4/1297.6	m/sh
$twCH_2$	1271.8	1.2	1287.8/1285.5	sh/w
δ(C–H P-ring 4)	1176.9	1.8	1177.2	w
δ(C–H P-ring 5)	1158.9	0.3	1161.5	w
$\gamma CH_3''/\gamma CH_2$	1150.0	3.6	1161.5	w
νN–N	1119.4	14.2	1135.7/1123.9	w/m
$\gamma CH_3'$	1103.0	39.1	1116.7	m
δ(C–C P-ring 6)	1089.5	5.5	1105.2/1099.5/ 1093.0	sh/w/w
δ(T-ring 2)	1064.4	85.8	1071.9/1070.1	m/sh
ν(C–C P-ring 5)	1041.8	9.7	1050.5/1047.6	sh/w
νC–C/νO–C	1017.5	95.8	1030.0/1026.0	S/sh
ν(C–C P-ring 1)/ δ(P-ring 1)	1014.0	11.2	1014.2	sh
ν(C–C P-ring 1)/δ(P-ring 1)	994.9	0.1	997.8	w
γ(C–H P-ring 5)	982.9	0.1	984.3	w
τ(T-ring 2)/νN–N'	974.1	5.0	978.3/973.8	w/w
τ(P-ring 3)/ γ(C–H P-ring 4)	966.1	0.1	978.3/973.8	w/w
γ(C–H P-ring 3)	909.9	4.7	911.1/910.2/907.2	w/w/sh
νO–C	889.6	32.8	902.9/901.0/ 900.0/886.3/884.9	w/w/w/w/w
γ(C–H P-ring 2)	830.5	0.1	829.7	w
$\gamma CH_3''/\gamma CH_2$	798.5	0.6	809.9	w
δ(T-ring 1)/νC–O / ν(C–C P-ring 1)	767.2	1.5	776.6/764.5	w/sh

Table 3. (Continued)[a]

γ(C–H P-ring 1)	754.1	59.2	757.0/755.4	m/m
τ(T-ring 2)/γCO	717.9	4.4	735.4/730.5	w/w
τ(P-ring 1)/τ(T-ring 1)	690.0	13.5	697.2/694.6	w/w
δ(P-ring 3)	681.5	15.0	685.7	m
τ(T-ring 1)	679.1	15.7	684.0/682.1/670.9	m/sh/w
δ(P-ring 2)	616.3	0.2	617.2	w
δCO/δNC	563.4	4.2	568.2	w
γNC	498.0	11.2	506.8	w
γ(C-H P-ring 4)/τ(P-ring3)	405.3	0.2		
δOCC/δCN	385.2	2.3		
γCO	353.5	4.2		
δOCC	325.0	5.6		
δCN/τ(T-ring 2)	298.5	2.3		
τ(P-ring 2)	258.2	0.7		
τCH_3	242.5	0.1	n.i.	n.i.
$\delta C–O–CH_3/\delta CN$	176.1	1.8		
γCN/τC–O	114.2	2.0		
τC–O	88.0	0.9		
δ(P-ring 1)/δNC/τC–O	76.2	0.4		
τO–C	58.1	0.9		
τC–N	29.1	0.8		

[a] ν, bond stretching; δ, bending; γ, rocking; τ, torsion; s, symmetric; as, antisymmetric; P-ring, phenyl ring; T-ring, tetrazole ring. See Table S9 (Appendix B) for definition of internal coordinates. S, strong; m, medium; w, weak, sh, shoulder; n.i., not investigated.

Conformer **T** belongs to the C_1 symmetry point group, with a dipole moment of 5.52 D and 66 fundamental vibrations, all of them predicted to be active in the infrared. In consonance with the spectral data previously obtained for a series of 1-phenyltetrazole-based compounds,[6,7,10,50] the IR spectrum of 5EPT can be considered as being constituted by two independent groups of bands, *i.e.,* one associated with the vibrational modes of the phenyl group and the other related with the tetrazole ring and ethoxy substituent.

The bands resulting from the first group show very small differences for 1-phenyltetrazole compounds; they appear in the spectrum of 5EPT at nearly the same frequencies as in 5-methoxy-1-phenyltetrazole[10] 1-phenyltetrazole,[6] 5-chloro-1-phenyltetrazole[6] and 1-phenyltetrazolone.[50] This result reinforces once again the idea that the presence of a second substituent at the tetrazole ring does not have a strong influence on the phenyl group, being also in consonance with the predicted small conjugation of the π electron systems of phenyl and tetrazole rings in 5EPT (also in

agreement with these results is the fact that the optimized structures of the various 1-phenyltetrazole compounds already studied,[6,7,10,51] including 5EPT, do not show any substantial differences in the geometry of the phenyl group).

As could be expected, and differing from what occurs for the phenyl vibrations, the tetrazole ring vibrations are strongly affected by the substituent at $C_{(5)}$ and differ considerably among different compounds. The most intense bands in the IR spectrum of 5EPT are associated with modes originated in this group, as well as in the ethoxy group, corresponding to the νC–O/νN=C, νC–N, νN=C/νN–C, νN–N, δ(T-ring 2), νC–C/νO–C, δCH_3 symmetric and ωCH_2 vibrational modes (see Table 3; and also Table S9 for definition of coordinates). The νC–O/νN=C vibrational mode, localized both in the $C_{(5)}$–$O_{(17)}$ and $C_{(5)}$–$N_{(4)}$ bonds, gives rise to the most intense band of the spectrum and occurs as a triplet at 1567.2/1565.2/1552.5 cm^{-1} (see Figure 8 and Table 3). In 5-methoxy-1-phenyltetrazole[10] the equivalent vibration absorbs as a site-split doublet at 1572.3 and 1571.3 cm^{-1}. The νC–N vibration (associated with the $C_{(5)}$–$N_{(1)}$ bond) gives rise to a doublet at 1453.0/1447.5 cm^{-1}, while that ascribable to the νN–C coordinate (associated with the $N_{(1)}$ –$C_{(6)}$ inter-ring bond) is observed as a doublet at 1299.4/1297.6 cm^{-1} (Table 3). According to the results of normal mode analysis [see Table S10 (Appendix B)] these coordinates are somewhat coupled with the *ν*N=C coordinate (specially the latter), what may justify their relatively high frequency. The νN–N vibrational mode, mainly localized in the $N_{(3)}$–$N_{(4)}$ bond, is observed as a doublet at 1135.7/1123.9 cm^{-1} (see Table S10). Another intense band in the spectrum of 5EPT is observed at 1071.9/1070.1 cm^{-1}, corresponding to the tetrazole ring δ(T-ring 2) vibration. In 5-methoxy-1-phenyltetrazole,[10] 1-phenyltetrazole and 5-chloro-1-phenyltetrazole,[6] the equivalent vibrations absorb at 1101.3/1096.9, 1089.5/1085.4 and 1109.1/1102.4 cm^{-1}, respectively, and are also comparable in intensity to the observed

band of 5EPT. The δCH_3 symmetric and ωCH_2 deformational modes of the ethyl group give rise also to relatively intense IR bands and appear as doublets at 1393.6/1388.5 and 1363.9/1360.6 cm^{-1}, respectively. Finally, the νC–C/νO–C mixed stretching mode is the last vibration among those giving rise to intense bands that were mentioned above. It is observed at 1030.0/1026.0 cm^{-1}, *i.e.* within the characteristic frequency range for this mode in methyl esters and methyl ethers (around 1050–950 cm^{-1}),[33] and at a similar value observed for 5MPT (1014.2/1011.5 cm^{-1}).

All the remaining intense bands in the IR spectrum of 5EPT belong to the phenyl moiety, being observed at 1509.5 cm^{-1} δ(C–H P-ring 2), 1462.3 cm^{-1} ν(C–H P-ring 3) and 757.0/755.4 cm^{-1} γ(C–H P-ring 1) (see Table 3).

▪ *In situ* UV-irradiation experiments (λ > 235 nm)

To study the photochemistry of the matrix-isolated 5EPT, *in situ* UV-irradiation (λ > 235 nm) experiments were carried out. The resulting photochemical processes were followed by IR spectroscopy. The interpretation of the experimental data was supported by extensive DFT calculations of the possible photoproducts and, whenever available, taking into consideration previously reported spectroscopic data obtained for putative photoproducts.

Upon irradiation, the bands due to 5EPT decrease in intensity, while new bands appear in the spectrum indicating that the compound is being transformed in other species. The changes are particularly evident in the 2300-1700 cm^{-1} spectral region, which is shown in Figure 9 (frame C: *spectrum of the photoproducts*).

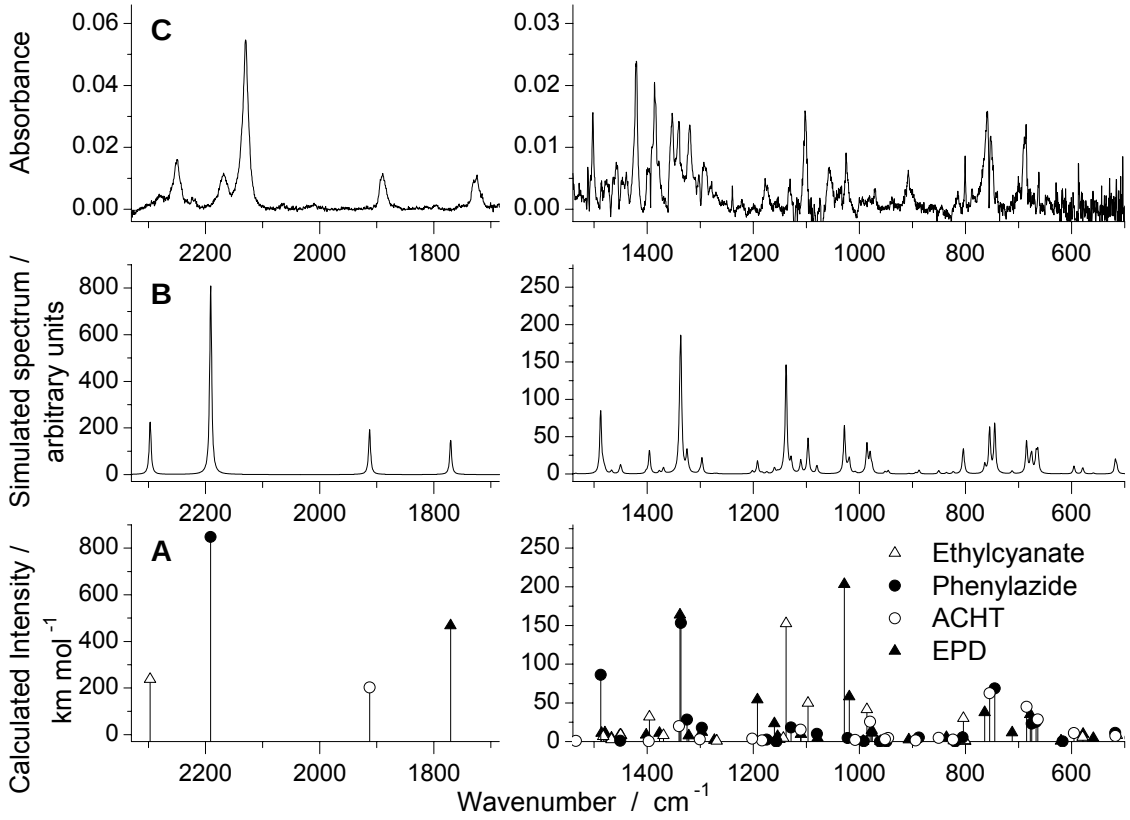

Figure 9. (**A**) DFT(B3LYP)/6-311++G(d,p) calculated spectra of the possible photoproducts: Δ – ethylcyanate (the most stable conformer **EC-A**); ● – Phenylazide; ○ – ACHT; ▲– EPD (most stable conformer **T-A**). The calculated wavenumbers were scaled with a uniform factor of 0.978. (**B**) Simulated infrared spectrum for the mixture of photoproducts. It was created using Lorentzian functions centered at the calculated (scaled) frequencies (shown in Frame A) and with bandwidths-at-half-height equal to 4 cm^{-1}. Note that the calculated intensities in the sum spectrum relate in the proportion 1:1:1:0.33, where 0.33 refers to EPD and unities refer to ethylcyanate, phenylazide and ACHT. (**C**) Extracted spectrum of the photoproducts formed after 60 minutes of UV-irradiation ($\lambda > 235$ nm) of 5EPT trapped in an Ar matrix. The extracted spectrum was obtained by subtraction of the scaled spectrum of non-irradiated matrix from the spectrum of irradiated sample. The scaling factor was chosen so that the absorptions due to the originally deposited compound (5EPT) were nullified.

The proposed reaction pathways resulting from irradiation of 5EPT are schematically shown in Figure 10, and the complete list of bands due to the products of photolysis is presented in Table 4.

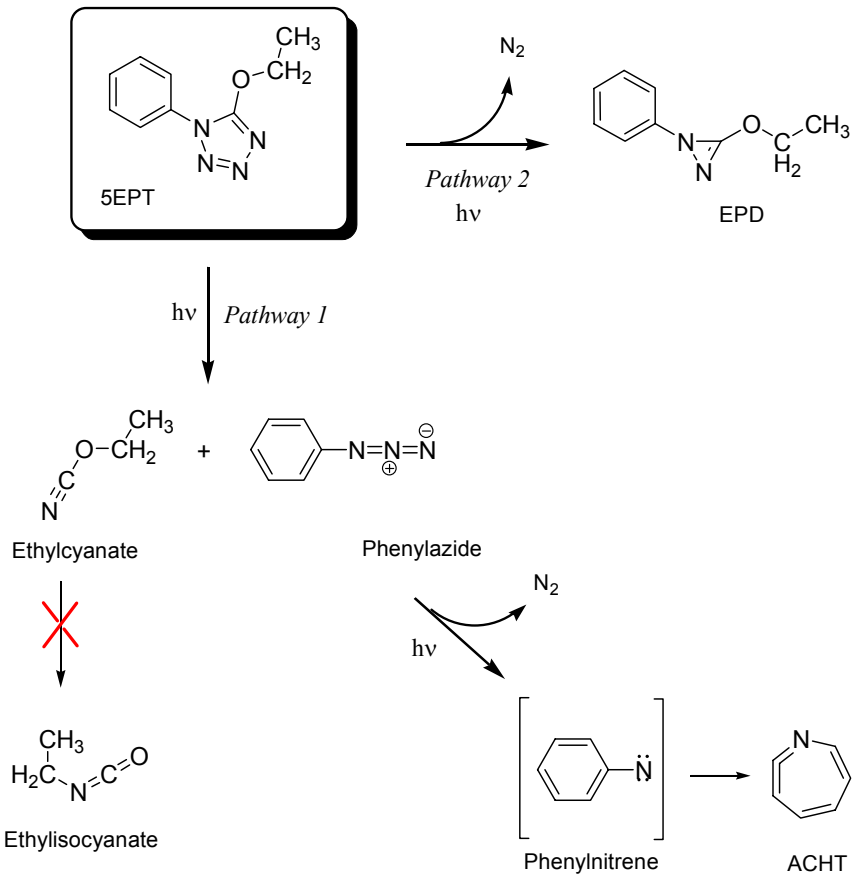

Figure 10. Proposed pathways resulting from irradiation of 5-ethoxy-1-phenyl-1*H*-tetrazole in an argon matrix through the outer KBr window of the cryostat ($\lambda > 235$ nm).

The observed photochemistry of 5EPT shows two major reaction pathways: *(1)* cleavage of the tetrazole ring through the $C_{(5)}$–$N_{(1)}$ and $N_{(3)}$–$N_{(4)}$ bonds, with production of phenylazide and ethylcyanate as primary photoproducts (phenylazide can then undergo further reactions to give 1-aza-1,2,4,6-cycloheptatetraene-ACHT), and *(2)* cleavage of the $N_{(1)}$–$N_{(2)}$ and $N_{(3)}$–$N_{(4)}$ bonds, with molecular nitrogen elimination, leading to formation of the antiaromatic 3-ethoxy-1-phenyl-1*H*-diazirene (EPD).

Table 4. Experimental and calculated [B3LYP/6-311++G(d,p); scaled by 0.978] vibrational frequencies (cm^{-1}) and calculated IR intensities (km mol^{-1}) for ethylcyanate, phenylazide and 1-aza-1,2,4,6-cycloheptatetraene (ACHT) (photoproducts formed by irradiation of 5-ethoxy-1-phenyl-1*H*-tetrazole in solid argon[a]).

Approximate Description[b]	Sym.	Calculated		Observed Frequency (cm^{-1})	Literature Frequency (cm^{-1})
		Frequency (cm^{-1})	Intensity (km mol^{-1})		
Ethylcyanate	C_s				*(gas phase)* [56]
νOCN as.	A'	2297.2	237.9	2251.2/2245.3	2262 /2255/2248
δCH_2	A'	1482.5	6.8	1480.0	1480
δCH_3 as'	A'	1467.2	2.8	1474.7	
δCH_3 as''	A''	1450.1	8.6	1439.6	1454
δCH_3 s	A'	1395.8	32.1	1386.2/1384.0	1401
ωCH_2	A'	1369.3	8.1	1379.6	1377
$twCH_2$	A''	1268.8	0.8	1287.0	1290
γCH_2	A''	1143.3	4.6	1136.6	1136
νOCN s	A'	1138.2	152.6	1133.8	1113
γCH_3'	A'	1096.8	49.9	1085.0	1106
νCC	A'	985.8	41.5	997.5/992.0	1008
νC–O	A'	804.0	30.2	805.6	825
γCH_3'	A''	801.2	1.3	800.8	814
δOCN	A'	579.3	5.9	596.8	-
Phenylazide	C_s				*(N_2 matrix)* [36]
νN=N=N as.	A'	2191.4	843.5	2168.7/2130.3	2165/2157/2137/2128[c] 2112/2102/2087
ν(C–C ring 2)	A'	1600.5	59.2	1621.1	1598
ν(C–C ring 4)	A'	1585.3	6.4	1579.7	1589/1585
δ(C–H ring 2)	A'	1487.7	86.3	1502.3	1496/1491
νN=N=N s.	A'	1336.4	151.2	1354.3/1352.7/1361.5	1398
δ(C–H ring 1)	A'	1325.0	29.8	1318.7	1337
ν(C–C ring 3)	A'	1296.8	18.2	1293.3	1305/1298
δ(C–H ring 4)	A'	1174.6	2.4	1174.4 (?)	1176
νN–C	A'	1128.9	18.3	1125.2	1136/1131
ν(C–C ring 5)	A'	1022.0	4.4	1025.2	1026
γ(C–H ring 3)	A''	887.7	5.2	886.5	896
δCNN	A'	805.5	5.3	814.0	810
γ(C–H ring 1)	A''	744.9	68.7	740.4	751
τ(ring 1)	A''	675.2	23.2	663.6	687
δNNN	A'	666.9	25.1	662.0	670
ACHT	C_1				*(Ar matrix)* [34]
νC=C=N as.		1913.1	202.2	1891.5	1895
δ(C–H 1)		1201.8	3.9	1222.3	
δ(C–H 2)		1110.9	15.2	1104.3/1102.3	1111
νN–C		979.7	25.6	970.4	980
γ(C–H 1)		951.4	3.0	939.4	940
γ(C–H 2)		945.7	4.5	935.4	
γ(C–H 3)		754.3	62.3	748.0	748
δCCN		685.0	45.5	689.7	683
τ(ring 1)		663.8	28.2	652.4	658/650
γCCN		595.5	10.9	586.4	580

[a] Complete calculated spectra are presented in Tables S5, S7, S13 and S14 (Appendix B).

[b] ν: stretching; δ: bending; γ: rocking; τ: torsion; tw: twisting; ring modes were given the names in consonance with those used for 5EPT. [c] Shoulder.

Both observed photoprocesses imply cleavage of the $N_{(3)}$–$N_{(4)}$ bond. The first one also implies disruption of the $C_{(5)}$–$N_{(1)}$ bond, while the second one requires cleavage of the $N_{(1)}$–$N_{(2)}$ bond. These are the three formally single bonds in the tetrazole ring, with calculated lengths longer than 135.7 pm [Table S8 (Appendix B)]. The $N_{(2)}$–$N_{(3)}$ and $C_{(5)}$–$N_{(4)}$ bonds are considerably shorter [128.0 and 131.4 pm, respectively, as calculated at the DFT(B3LYP)/6-311++G(d,p) level of theory], and represent the two double bonds of tetrazolic system. Thus, the bonds that undergo cleavage in the photoreactions correspond to the tetrazole ring weaker bonds, as it was also found for the closely related molecule 5-methoxy-1-phenyltetrazole.[10]

As could be expected, and also similarly to what was previously observed for 5MPT, the first observed photoprocess is clearly the preferred reaction channel in 5EPT, as can be noticed by comparing the relative intensities of the mark bands due to the different photoproducts appearing in the 2300-1700 cm^{-1} spectral range.

As already mentioned, all strong and medium intensity bands predicted for the two major products formed in *Pathway 1* (phenylazide and ethylcyanate) could be observed in the spectra of the irradiated matrix (see Figure 9 and Table 4).

Covalent cyanates (R–O–C≡N) are in general unstable compounds and isomerize into their thermodynamically more stable isocyanate derivatives. The cyanate structure is stable only in special cases, *e.g.,* if the substituent, R, is an aryl group,[57,58] or if the substituent is bulky, preventing the isomerization for sterical reasons.[59,60] Ethylcyanate, CH_3CH_2OCN, is not an exception. It isomerizes readily at room or higher temperatures,[61] and the process is believed to be autocatalyzed.[58] Because of its instability, ethylcyanate can only be stored at low temperature and its application in chemical reactions requires its generation *in situ* prior to use.[62-64] For the same reason, little is known experimentally about ethylcyanate structure and spectroscopy. The

IR[65,66] and NMR[65] spectra of the compound were recorded in cold CCl_4 solution. Gas-phase investigations on this substance include only early mass[67] and microwave[56] spectroscopic studies. More recently, gaseous ethylcyanate, has been generated from the gas/solid reaction of *o*-ethyl thiocarbamate with mercury oxide, and characterized in the gas phase by infrared spectroscopy.[36]

In the present study, all bands previously observed in the gas phase spectrum of ethylcyanate[56] could be identified in the spectra of the irradiated matrix (Table 4), unequivocally testifying the presence of this species. Like observed before for methylcyanate resulting from photolysis of 5MPT, no evidence for isomerization of ethylcyanate to ethylisocyanate was found, indicating that, under the experimental conditions used, ethylcyanate is stable in relation to the isomerization to the isocyanate.

It is worth noticing that ethylcyanate has one intramolecular degree of freedom, corresponding to internal rotation around the $-C_{(4)}-O-$ bond [see Table S13 (Appendix B)], which may result in the existence of different conformers. The potential energy profile for internal rotation around the $-C_{(4)}-O-$ bond in ethylcyanate (see Figure 11) was calculated by incrementing the value of the C−C−O−C dihedral angle and fully optimizing all other geometric parameters. This relaxed potential energy scan confirmed the existence of three local minima, which are associated with conformers **T**, **G** and **G'** (structures **G** and **G'** are mirror images). The energy barrier separating the **G** and **G'** forms from the most stable form **T** is very low, amounting to less than 4 kJ mol^{-1}. The optimized geometries of these conformers were obtained at the DFT(B3LYP)/6-311++G(d,p) level of theory and are depicted graphically in Tables S13 and S14 (Appendix B). Similarly to the matrix-isolated 5EPT, the photochemically produced ethylcyanate can also be expected to undergo conformational cooling, since the barrier

to intramolecular rotation remains low in this species. This justifies the sole observation in the irradiated matrices of the **T** conformer.

In *Pathway 1*, phenylazide is produced together with ethylcyanate (Figure 10). Phenylazide has been previously isolated and irradiated in argon matrix, and the production of 1-aza-1,2,4,6-cycloheptatetraene (ACHT) unequivocally demonstrated.[50] The vibrational spectra of matrix isolated phenylazide[34] and of ACHT[68] are thus well known and their identification could be made here without any difficulty (see Table 4). Under the experimental conditions used, phenylazide reacts with relatively low efficiency, in particular when compared to the reactions undergone by the tetrazole compounds. The intermediate for this reaction is, with all probability, the singlet phenylnitrene, which has been found to easily undergo ring expansion to ACHT (the calculated ground state energies for these two species favour the latter compound by *ca.* 80 kJ mol^{-1}).

Characteristic bands of ACHT[50] were clearly identified in the spectra of the irradiated matrix. Particularly evident is the band-mark associated with the intense antisymmetric stretching vibration of the ketenimine moiety (νC═C═N as.) of ACHT, observed at 1891.5 cm^{-1} (Figure 9). Other bands previously described as fingerprints for this compound could also be clearly identified in the spectra (Table 4).

Note also that, as found previously for UV-irradiation of 5-methoxy-1-phenyltetrazole[10] and 1-phenyltetrazolone monomers isolated in argon,[50] triplet phenylnitrene (reported to be present in low temperature matrices as a result of direct photolysis of isolated phenylazide[40]) was not observed in the present study. Like previously suggested,[10,50] the absence of observation of triplet phenylnitrene may result from the fact that phenylazide is produced together with other species and might interact

with them in the matrix cage, eventually making inaccessible the pathway which would lead to formation of the triplet nitrene.

In reaction *Pathway 2*, the extrusion of molecular nitrogen from the tetrazole ring leads to formation of a three-membered heterocyclic ring, namely 3-ethoxy-1-phenyl-1*H*-diazirene (EPD, Figure 10), which to the best of our knowledge was never described before. The elimination of molecular nitrogen after irradiation of tetrazole compounds to give diazirenes has already been described.[6,50] As already mentioned, diazirenes can be easily identified because their most intense band (νC=N) occurs in a "clean" region of the spectrum (1850–1720 cm^{-1}), appearing as a suitable fingerprint for this family of compounds. In the spectra of the irradiated matrix, the band corresponding to this vibration was clearly identified at 1725 cm^{-1} (see Table 5 and Figure 9).

Similarly to the general picture described above for ethylcyanate, three conformers (**T**, **G**, **G'**) separated by low intramolecular energy barriers (less than 3 kJ mol^{-1}) were also predicted by the calculations for EPD. The potential energy profile for internal rotation around the $-C_{(4)}-O-$ bond in EPD is shown in Figure 11 along with that for ethylcyanate. The optimized geometries of the three conformers of EPD, calculated at the DFT(B3LYP)/6-311++G(d,p) level of theory, are included in Tables S15-S17 (Appendix B). Once again, conformational cooling took place with these species, leading to the exclusive observation of the most stable **T** conformer and thus facilitating the interpretation of the photo-processes occurring in the matrix.

Table 5. Experimental and calculated [B3LYP/6-311++G(d,p); Scaled by 0.978] vibrational frequencies (cm^{-1}) and calculated IR intensities (km mol^{-1}) for 3-ethoxy-1-phenyl-1*H*-diazirene (EPD) (photoproduct formed by irradiation of 5-ethoxy-1-phenyl-1*H*-tetrazole in solid argon[a]).

Approximate Description[b]	Calculated		Observed Frequency (cm^{-1})
	Frequency (cm^{-1})	Intensity (km mol^{-1})	
EPD			
νC=N	1770.4	468.2	1724.5
δ(C−H ring 2)	1594.1	0.5	1572.7
δ(C−H ring 1)	1579.0	0.5	1572.7
δCH_2	1486.0	10.9	1480.0[c]
δ(C−H ring 4)	1479.7	11.6	1477.5
δCH_3 as.'	1467.2	4.9	1474.7[c]
γCH_3'	1451.9	8.2	1445.6/1439.6
δ(C−H ring 5)	1448.6	7.8	1425.6/1420.2
ωCH_2	1401.9	8.5	1348.8/1346.9
δCH_3 s	1377.1	10.8	1388.1
δCN	1338.0	163.6	1324.2
δ(C−H ring 2)	1321.7	7.7	1322.0
δ(C−H ring 1)	1296.9	12.2	1293.3[d]
$twCH_2$	1273.3	1.8	1278.8
δ(C−H ring 4)	1192.0	54.2	1177.4
δ(C−H ring 5)	1160.2	23.4	1174.4[d]
ν(C−C ring 5)	1154.1	6.8	1133.6
$twCH_2$	1150.6	3.2	1133.6
γCH_3'	1110.2	9.5	1111.2
ν(C−C ring 5)	1079.0	4.6	1082.8
$\nu O–C(H_2)$	1028.3	203.2	1055.9
γ(C−H ring 3)	1019.1	58.1	1025.2[d]
ν(C−C ring 5)	992.8	0.7	n.o.[e]
γ(C−H ring 5)	976.5	14.6	970.4
γ(C−H ring 1)	976.0	11.1	970.4
γ(C−H ring 2)	960.1	0.5	959.8
γ(C−H ring 4)	906.9	2.5	886.5[d]
νC-O	835.9	5.7	833.2
γ(C−-H ring 1)	822.1	1.1	821.0
γ(NN(C)O)[f]	806.0	4.8	805.6[c]
γCH_3'	800.5	0.7	800.8[c]
τ(ring 1)	763.8	37.7	788.8/784.7
τ(ring 2)	712.2	11.5	735.6
τ(ring 3)	677.7	35.2	682.2

[a] Complete calculated spectra are presented in Tables S15-S17 (Appendix B).

[b] ν: stretching; δ: bending; γ: rocking; τ: torsion; tw: twisting; ring modes were given the names in consonance with those used for 5EPT. [c] Overlapped with a band of ethylcyanate.

[d] Overlapped with a band of phenylazide.

[e] n.o., not observed.

[f] C out of the N–N–(C)–O plane bending vibration.

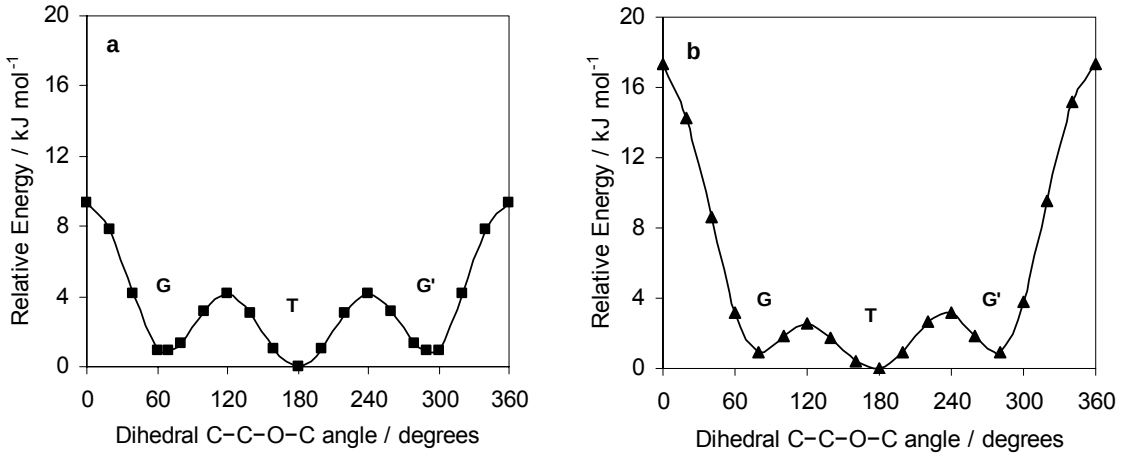

Figure 11. DFT(B3LYP)/6-311++G(d,p) calculated potential energy profiles for internal rotation of the ethoxy group around the $C_{(4)}$–$O_{(1)}$ bond in ethylcyanate (EC; *frame* **a**) and 3-ethoxy-1-phenyl-1*H*-diazirene (EPD; *frame* **b**). The energy of the conformers **T** (the lowest-energy structures) is equal to −247.338011 and −533.742444 hartree for EC and EPD respectively (without the ZPE contribution) and was chosen as the relative zero level. Minima denoted as **G**, **T** and **G'** on the curves, correspond to the lower energy conformers (Tables S13-S17, Appendix B).

▪ Conclusions

DFT(B3LYP)/6-311++G(d,p) calculations performed in this study predict that, in the gaseous phase, 5EPT should exist in three different conformers. However, only the most stable of these forms was observed for the compound isolated in an argon matrix at 12 K. The potential energy profile for the internal rotation of the ethyl group in 5EPT was calculated, revealing that the energy barriers separating the two minima of higher energy from the most stable form are very low (less than 4 kJ mol^{-1}). These barriers are readily surpassed during deposition of 5EPT into the argon matrix (conformational cooling) justifying the sole conformer of 5EPT retained in the sample. After UV irradiation (λ > 235 nm) of the matrix, two different reaction pathways could be identified, both corresponding to cleavage of the tetrazole ring: *Pathway 1*: production of phenylazide and ethylcyanate as primary photoproducts, and *Pathway 2*: molecular nitrogen elimination, leading to formation of the antiaromatic 3-ethoxy-1-phenyl-1*H*-diazirene (EPD). The primarily formed phenylazide (*Pathway 1*) is partially

converted into 1-aza-1,2,4,6-cycloheptatetraene (ACHT), with all probability involving the singlet phenylnitrene as intermediate. The identification of the photoproducts was carried out taking into account both the theoretical spectra for the different putative products and the available literature data on those compounds. The conformational cooling occurrence verified during this work – relaxation of the high energy forms of both reagent (5EPT) and products (ethylcyanate and EPD) into their lower energy structures –, facilitated the interpretation of the processes taking place in the matrix, enabling to attain a high degree of certainty in the identification and characterization of the different photoproducts.

3.1.4. Experimental Section

Equipment and experimental conditions. All chemicals were used as purchased from Aldrich. Solvents for extraction and chromatography were of technical grade. When required, the solvents used in reactions were freshly distilled from appropriate drying agents before use. Analytical TLC was performed with Merck silica gel 60 F_{254} plates. Melting points were recorded on a Stuart Scientific SMP3 melting point apparatus and are uncorrected. Mass spectra were obtained on a VG 7070E mass spectrometer by electron ionization (EI, 70 eV). ^{1}H NMR (400 MHz) spectra were obtained on a Bruker AM-400 spectrometer using TMS the internal reference (δ = 0.0 ppm).

Infrared spectroscopy. The IR spectra were obtained using a Mattson (Infinity 60AR Series) Fourier Transform infrared spectrometer, equipped with a deuterated triglycine sulphate (DTGS) detector and a Ge/KBr beamsplitter, with 0.5 cm^{-1} spectral resolution. In order to avoid interference from atmospheric H_2O and CO_2, a stream of dry nitrogen continuously purged the optical path of the spectrometer. The compound was placed in a specially designed doubly thermostattable Knudsen cell,[69] whose compartments (sample container and valve nozzle) were kept at 323 K (for 5MPT) or 333 K (for 5EPT) during deposition of the matrix. Matrices were prepared by co-deposition, onto the CsI substrate of the cryostat cooled to 9 K (for 5MPT) or 12 K (for 5EPT), of compound vapors coming out of the Knudsen cell and a large excess of the matrix gas (argon N60, Air Liquide) coming from a separate line. All experiments were performed using an APD Cryogenics closed-cycle helium refrigeration system with a DE-202A expander.

Irradiation of the samples was carried out with a 150W xenon arc lamp (Osram XBO 150W/CR OFR), through the outer KBr window of the cryostat ($\lambda > 235$ nm).

Computational methodology. The quantum chemical calculations of the stationary points were performed at the DFT level of theory using the standard 6-311++G(d,p) basis set and the three-parameter density functional abbreviated as B3LYP, which includes Becke's gradient exchange correction[70] and the Lee, Yang, Parr correlation functional.[71] Structural results for 5MPT and 5EPD are provided in Tables S1 and S8 (Appendix B) respectively. Potential energy scans were performed using the 6-31G(d,p) basis set. The nature of the obtained stationary points was checked through the analysis of the corresponding Hessian matrix.

DFT(B3LYP)/6-311++G(d,p) harmonic vibrational frequencies and IR intensities were calculated at the optimized geometries. To correct the systematic shortcomings of the applied methodology (mainly for anharmonicity), the predicted vibrational wavenumbers were scaled down by a single factor of 0.978. The theoretical normal modes, calculated for 5MPT and conformers of 5EPT (**T**, **G** and **G'**), were analyzed by calculating their potential energy distributions (PED) in the molecule-fixed internal coordinates system as described by Schachtschneider.[72] The internal coordinates used in this analysis were defined following the recommendations of Pulay *et al.*,[73] and are listed in Tables S2 and S9 (Appendix B). The elements of potential energy distribution (PED) matrices are given in Tables S3 and S10-S12 (Appendix B). All calculations in this work were carried out using the Gaussian 03 program.[74]

Synthesis of 5-alkoxy-1-phenyl-1*H*-tetrazoles.

Diverse methodologies to synthesize 5-alkoxy- and 5-aryloxy-1-aryl tetrazoles have been described[2,75] in view of the great importance of these compounds, from a synthetic point of view, as intermediates to the preparation of 1-alkyl-4-aryl-4,5-dihydro-1*H*-tetrazol-5-ones *via* a thermally-induced Chapman isomerization.[3,4] In the present study, 5MPT and 5EPT were prepared by a novel method, described below.

General procedure for the preparation of 5-methoxy-1-phenyl-1*H*-tetrazole (5MPT) and 5-ethoxy-1-phenyl-1*H*-tetrazole (5EPT).

5-Methoxy-1-phenyl-1*H*-tetrazole (5MPT). Small fragments of metallic sodium (Na(s), 1 g; 43 mmol) were added carefully to dry methanol (50 mL). The mixture was stirred at room temperature under an argon atmosphere until the effervescence had ceased (10 min). 5-Chloro-1-phenyl-1*H*-tetrazole (1.3 g; 7.2 mmol) in dry methanol (20 mL) was added and the mixture was stirred overnight at room temperature. The reaction was monitored by TLC using a mixture of dichloromethane/hexane (2:1) as eluent. The deposited white precipitate was filtered and washed with ethyl acetate (50 mL). Ice-water (50 mL) was added to the combined organic extracts and the organic product extracted with ethyl acetate (3 × 50 mL). The organic phase was dried (Na_2SO_4) and evaporated to dryness to give 5-methoxy-1-phenyl-1*H*-tetrazole as a white solid (1.0 g; 79% yield), mp 42-43°C. ^{1}H NMR ($CDCl_3$): δ 3.92-3.99 (3H, s), 7.40-7.45 (1H, t), 7.49-7.54 (2H, t), 7.69-7.71 (2H, d) ppm; MS (EI), *m*/*z* 177 $[M+H]^+$.

Similarly, 5EPT was prepared.

5-Ethoxy-1-phenyl-1*H*-tetrazole (5EPT). Reaction in dry ethanol. Product obtained as a white solid (1.2 g; 88% yield), mp 52-53°C. ^{1}H NMR ($CDCl_3$): δ 1.52-1.56 (3H, t), 4.69-4.74 (2H, q), 7.43-7.47 (1H, t), 7.51-7.55 (2H, t), 7.72-7.74 (2H, d) ppm; MS (EI), *m*/*z* 191 $[M+H]^+$.

[See ^{1}H-NMR data of 5EPT at pages S1(B)-S3(B), Appendix B].

3.1.5. References

1. Smirnova, G. G.; Kovaleva, O. P.; Artamova, T. V.; Koreneva, A. P.; Koldobskii, G. I. *Russ. J. Org. Chem.* **2003**, *39*, 1679.
2. Demko, Z. P.; Sharpless, K. B. *Angew. Chem.-Int. Edit.* **2002**, *41*, 2110.
3. Vollmar, A.; Hassner, A. *J. Heterocycl. Chem.* **1974**, *11*, 491.
4. Cristiano, M. L. S. *PhD. Thesis*, University of Liverpool, 1994.
5. Bugalho, S. C. S.; Maçôas, E. M. S.; Cristiano, M. L. S.; Fausto, R. *Phys. Chem. Chem. Phys.* **2001**, *3*, 3541.
6. Bugalho, S. C. S.; Lapinski, L.; Cristiano, M. L. S.; Frija, L. M. T.; Fausto, R. *Vibrat. Spectrosc.* **2002**, *30*, 213.
7. Bugalho, S. C. S.; Serra, A. C.; Lapinski, L.; Cristiano, M. L. S.; Fausto, R. *Phys. Chem. Chem. Phys.* **2002**, *4*, 1725.
8. Gómez-Zavaglia, A.; Reva, I. D.; Frija, L.; Cristiano, M. L.; Fausto, R. *J. Phys. Chem. A* **2005**, *109*, 7967.
9. Gómez-Zavaglia, A.; Reva, I. D.; Frija, L.; Cristiano, M. L.; Fausto, R. *J. Mol. Struct.*, **2006**, *786*, 182.
10. Gómez-Zavaglia, A.; Reva, I. D.; Frija, L.; Cristiano, M. L. S.; Fausto, R. *J. Photochem. Photobiol. A-Chem.* **2006**, *180*, 175.
11. Maier, G.; Eckwert, J.; Bothur, A.; Reisenauer, H. P.; Schmidt, C. *Liebigs Ann.* **1996**, 1041.
12. Dunkin, I. R.; Shields, C. J.; Quast, H. *Tetrahedron* **1989**, *45*, 259.
13. Chae, Y. B.; Chang, K. S.; Kim, S. S. *The Daehan Hwak Hwoejee* **1967**, *11*, 85.
14. Awadallah, A.; Kowski, K.; Rademacher, P. *J. Heterocycl. Chem.* **1997**, *34*, 113.
15. Cristiano, M. L. S.; Johnstone, R. A. W. *J. Chem. Res. (Synopses)* **1997**, *5*, 164.
16. Hargreaves, A.; Rizvi, S.H. *Acta Cryst.* **1962**, *15*, 365.
17. Suzuki, H. *Bull. Chem. Soc. Jpn.* **1959**, *32*, 1340.
18. Beaven, G.H. in: Gray, G.W. (Ed.), *Steric Effects in Conjugated Systems*, Butterworths, London, 1958.
19. Ribeiro da Silva, M. A. V.; Matos, M. A. R.; Rio, C. A.; Morais, V. M. F.; Wang, J.; Nichols, G.; Chickos, J. S. *J. Phys. Chem. A* **2000**, *104*, 1774.
20. Catalan, J.; dePaz, J. L. G.; delValle, J. C.; Kasha, M. *J. Phys. Chem. A* **1997**, *101*, 5284.
21. Lynch, D. E.; McClenaghan, I. *Acta Crystallogr. Sect. E.-Struct Rep. Online* **2001**, *57*, 264.
22. Damrauer, N. H.; McCusker, J. K. *J. Phys. Chem. A* **1999**, *103*, 8440.
23. Cyranski, M. K.; Mieczkowski, J. *Acta Crystallogr. Sect. C-Cryst. Struct. Commun.* **1998**, *54*, 1521.
24. Matsunaga, T.; Ohno, Y.; Akutsu, Y.; Arai, M.; Tamura, M.; Iida, M. *Acta Crystallogr. Sect. C-Cryst. Struct. Commun.* **1999**, *55*, 129.
25. Zukermanschpector, J.; Barreiro, E. J.; Freitas, A. C. C. *Acta Crystallogr. Sect. C-Cryst. Struct. Commun.* **1994**, *50*, 2095.
26. Kowalski, A. *Acta Crystallogr. Sect. C-Cryst. Struct. Commun.* **1995**, *51*, 1670.
27. Damrauer, N. H.; Weldon, B. T.; McCusker, J. K. *J. Phys. Chem. A* **1998**, *102*, 3382.
28. Batista de Carvalho, L. A. E.; Teixeira-Dias, J. J. C.; Fausto, R. *Struct. Chem.* **1990**, *1*, 533.
29. Pearson, R.; Lovas, F. J. *J. Chem. Phys.* **1977**, *66*, 4149.
30. Cradock, S.; Purves, C.; Rankin, D. W. H. *J. Mol. Struct.* **1990**, *220*, 193.

31. Fernholt, L.; Romming, C. *Acta Chemica Scandinavica Series a-Physical and Inorganic Chemistry* **1978**, *32*, 271.
32. Bormans, B. J. M.; Dewith, G.; Mijlhoff, F. C. *J. Mol. Struct.* **1977**, *42*, 121.
33. Teixeira-Dias, J. J. C.; Fausto, R. *J. Mol. Struct.* **1986**, 199.
34. Jensen, K. A.; Due, M.; Holm, A. *Acta Chem. Scand.* **1965**, *19*, 438.
35. Martin, D.; Mucke, W. *Chem. Ber.* **1965**, *98*, 2063.
36. Pasinszki, T.; Westwood, N.P.C. *J. Phys. Chem.* **1995**, *99*, 1649.
37. Faustov, V. I.; Baskir, E. G.; Biryujov, A. A. *Russ. Chem. Bull., Intl. Edition* **2003**, *52*, 2328. (Published also in Russian in *Izv.Akad.Nauk., Ser. Kimicheskaya* **2003**, *11*, 2203.)
38. Chapman, O. L.; Roux, J.-P. *J. Am. Chem. Soc.* **1978**, *100*, 282.
39. Dunkin, I. *Spectrochim. Acta.* **1986**, *42*, 649.
40. Hayes, J. C.; Sheridan, R. S. *J. Am. Chem. Soc.* **1990**, *112*, 5879.
41. Otsuka, S.; Nakamura, A.; Yoshida, T. J. *Organometallic Chem.,* **1967**, *7*, 339.
42. Huisgen, R.; Vossius, D.; Appl, M. *Chem. Ber.* **1958**, *91*, 1 and **1958**, *91*, 12.
43. Barnes, A. J. *J. Mol. Struct.* **1984**, *113*, 161.
44. Jesus, A. J. L.; Rosado, M. T. S.; Reva, I.; Fausto, R.; Eusébio, M. E.; Redinha, J. S. *J. Phys. Chem. A* **2006**, *110*, 4169.
45. Reva, I.; Simao, A.; Fausto, R. *Chem. Phys. Lett.* **2005**, *406*, 126.
46. Reva, I. D.; Jesus, A. J. L.; Rosado, M. T. S.; Fausto, R.; Eusebio, M. E.; Redinha, J. S. *Phys. Chem. Chem. Phys.* **2006**, *8*, 5339.
47. Reva, I. D.; Stepanian, S. G.; Adamowicz, L.; Fausto, R. *Chem. Phys. Lett.* **2003**, *374*, 631.
48. Borba, A.; Gómez-Zavaglia, A.; Fausto, R. *J. Mol. Struct.* **2006**, *794*, 196.
49. Borba, A.; Gómez-Zavaglia, A.; Simões, P. N. N. L.; Fausto, R. *J. Phys. Chem. A* **2005**, *109*, 3578.
50. Gómez-Zavaglia, A.; Reva, I. D.; Frija, L.; Cristiano, M. L.; Fausto, R. *J. Photochem. Photobiol. A-Chem.* **2006**, *179*, 243.
51. Quast, H.; Bieber, L. *Angew. Chem.-Int. Edit. Engl.* **1975**, *14*, 428.
52. Quast, H.; Bieber, L. *Chem. Ber.-Recl.* **1981**, *114*, 3253.
53. Quast, H.; Fuss, A.; Nahr, U. *Chem. Ber.-Recl.* **1985**, *118*, 2164.
54. Quast, H.; Nahr, U. *Chem. Ber.-Recl.* **1985**, *118*, 526.
55. Quast, H. *Heterocycles* **1980**, *14*, 1677.
56. Sakaizumi, T.; Mure, H.; Ohashi, O.; Yamaguchi, I. *J. Mol. Spectrosc.* **1989**, *138*, 375.
57. Patai, S. *The Chemistry of Cyanates and their Thio Derivatives*; Ed.; Wiley: New York, 1977.
58. Martin, D.; Niclas, H. J.; Habisch, D. *Annalen Der Chemie-Justus Liebig* **1969**, *727*, 10.
59. Aljuaid, S. S.; Alnasr, A. A. K.; Ayoko, G. A.; Eaborn, C.; Hitchcock, P. *J. Organomet. Chem.* **1995**, *488*, 155.
60. Eaborn, C.; Lickiss, P. D.; Marquinachidsey, G.; Thorli, E. Y. *J. Chem. Soc.-Chem. Commun.* **1982**, 1326.
61. Martin, D. *Tetrahedron Lett.* **1964**, 2829.
62. Martin, D.; Weise, A. *Chem. Ber.-Recl.* **1966**, *99*, 976.
63. Holm, A.; Hugejens.E. *Acta Chemica Scandinavica Series B-Organic Chemistry and Biochemistry* **1974**, *B 28*, 705.
64. Fischer, H.; Zeuner, S.; Ackermann, K.; Schubert, U. *J. Organomet. Chem.* **1984**, *263*, 201.
65. Groving, N.; Holm, A. *Acta Chem. Scand.* **1965**, *19*, 443.

66. Reich, P.; Martin, D. *Chem. Ber.-Recl.* **1965**, *98*, 2063.
67. Jensen, K. A.; Holm, A.; Wentrup, C. *Acta Chem. Scand.* **1966**, *20*, 2107.
68. Teixeira-Dias, J. J. C.; Fausto, R. *J. Mol. Struct.* **1986**, *144*, 199.
69. Reva, I. D.; Stepanian, S. G.; Adamowicz, L.; Fausto, R. *J. Phys. Chem. A* **2001**, *105*, 4773.
70. Becke, A. D. *Phys. Rev. A* **1988**, *38*, 3098.
71. Lee, C. T.; Yang, W. T.; Parr, R. G. *Phys. Rev. B* **1988**, *37*, 785.
72. Schachtschneider, J. H. "Technical Report, Shell Development Co. Emeryville, CA,", 1969.
73. Pulay, P.; Fogarasi, G.; Pang, F.; Boggs, J. E. *J. Am. Chem. Soc.* **1979**, *101*, 2550.
74. Frisch, M.J.; Trucks, G.W.; Schlegel, H.B.; Scuseria, G.E.; Robb, M.A.; Cheeseman, J.R.; Montgomery, J.A.; Vreven, T.; Kudin, K.N.; Burant, J.C.; Millam, J.M.; Iyengar, S.S.; Tomasi, J.; Barone, V.; Mennucci, B.; Cossi, M.; Scalmani, G.; Rega, N.; Petersson, G.A.; Nakatsuji, H.; Hada, M.; Ehara, M.; Toyota, K.; Fukuda, R.; Hasegawa, J.; Ishida, M.; Nakajima, T.; Honda, Y.; Kitao, O.; Nakai, H.; Klene, M.; Li, X.; Knox, J.E.; Hratchian, H.P.; Cross, J.B.; Bakken, V.; Adamo, C.; Jaramillo, J.; Gomperts, R.; Stratmann, R.E.; Yazyev, O.; Austin, A.J.; Cammi, R.; Pomelli, C.; Ochterski, J.W.; Ayala, P.Y.; Morokuma, K.; Voth, G.A.; Salvador, P.; Dannenberg, J.J.; Zakrzewski, V.G.; Dapprich, S.; Daniels, A.D.; Strain, M.C.; Farkas, O.; Malick, D.K.; Rabuck, A.D.; Raghavachari, K.; Foresman, J.B.; Ortiz, J.V.; Cui, Q.; Baboul, A.G.; Clifford, S.; Cioslowski, J.; Stefanov, B.B.; Liu, G.; Liashenko, A.; Piskorz, P.; Komaromi, I.; Martin, R.L.; Fox, D.J.; Keith, T.; Al-Laham, M.A.; Peng, C.Y.; Nanayakkara, A.; Challacombe, M.; Gill, P.M.W.; Johnson, B.; Chen, W.; Wong, M.W.; Gonzalez, C.; Pople, J. A. Gaussian 03, Revision C.02 ed.; Gaussian, Inc.: Wallingford CT, 2004.
75. Smirnova, G. G.; Kovaleva, O. P.; Artamonova, T. V.; Koreneva, A. P.; Koldobskii, G. I. *Russ. J. Organ. Chem.* **2003**, *39*, 1679.